Chapter I

Hydrodynamic models and their implications in the transient and residual circulations, mud deposition and soil erosion, chemical and ecological dynamics in the Southern Bight of the North Sea

by

Jacques C.J. NIHOUL

Based on work by ADAM Y., DE BACKER J.L., LAMBERMONT J., LEBON G., NIHOUL J.C.J., RONDAY F.C.
Geophysical Fluid Dynamics Groups, Universities of Liège and Louvain.

This chapter is a synthesis of recent advances of the Math. Modelsea programme prepared as a working document for internal circulation and for presentation to the International Council for the Exploration of the Sea. The material is taken from recent progress reports and published papers and books. References should be made to the original publications.

I.- *THE SOUTHERN BIGHT MODEL IN THE NORTH SEA MODELLING EFFORT*

Based on :

- Math. Modelsea (1974), I.C.E.S. Hydrography Committee, C.M. 1974 - C : 1;
- NIHOUL J.C.J. (1975a), Modelling of Marine Systems, Elsevier Publ., Amsterdam;
- NIHOUL J.C.J. (1975b), Application of Mathematical Models to the Study, Monitoring and Management of the North Sea, in "Ecological Modelling in a Resource Management Framework", Resources for the Future, Washington D.C.

Mathematical models of the North Sea have been developed in most of the bordering countries. The national efforts are now coordinated by the Joint North Sea Modelling Group initiated by JONSIS (the Joint North Sea Information System) reporting to I.C.E.S. (the International Council for Exploration of the Sea). Data are provided by international surveys called JONSDAP (Joint North Sea Data Acquisition Program).

In an earlier stage, the models tended to address separately the Physics, the Chemistry and the Biology of the North Sea. Now, the development of computing facilities allowing more ambitious programs, these models are progressively integrated in a common, general, interdisciplinary model with the purpose of understanding the North Sea environment, predicting its evolution, — taking into account the constraints of modern society — , and assisting its management.

The distinction, between complex research models and simple, oriented management models, is avoided. Management models are regarded as "subsets" of the general multipurpose model, derived from it to answer specific questions with the degree of sophistication which the objectives, on the one hand, the reliability of data, on the other hand, recommend.

The different stages in the elaboration of the mathematical model and of its submodels are shown in figure 1.

1.-

The mathematical description of the system is confronted with the data base constituted from existing or newly acquired data (*e.g.* Jonsdap campaigns, Belgian five years' survey of the Eastern part of the Southern Bight, ...). The data base provides information for :

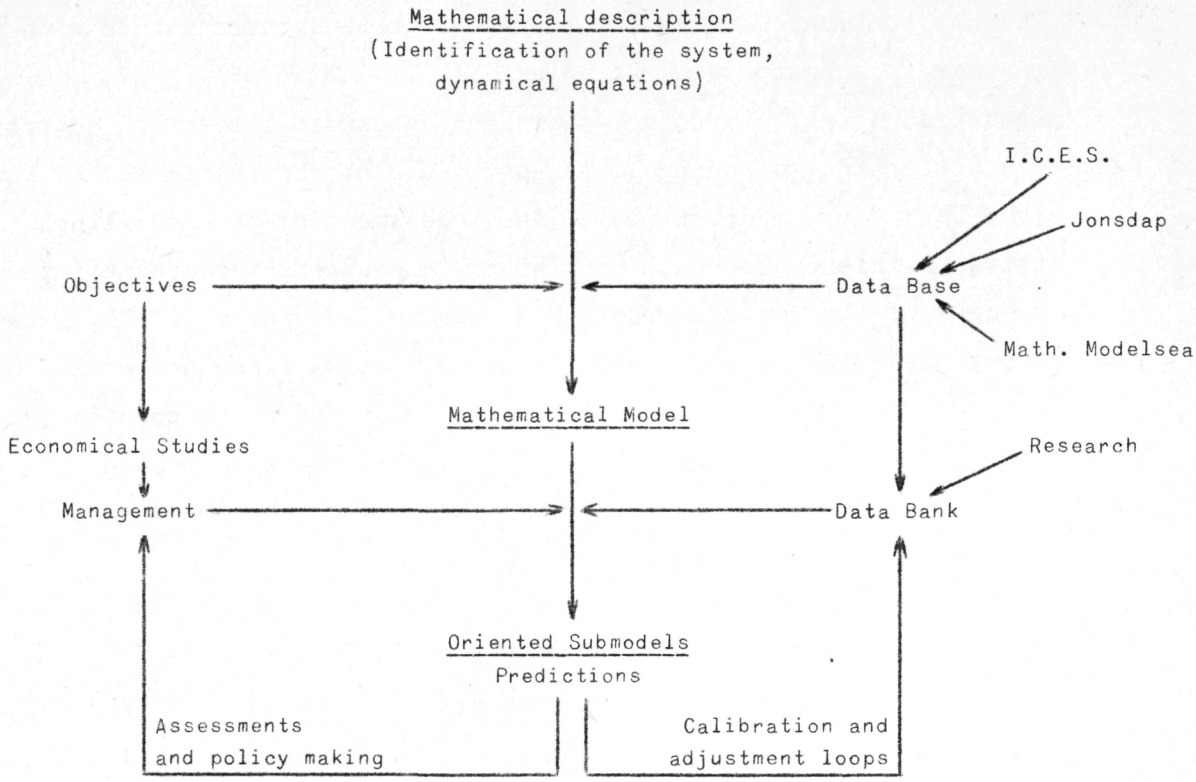

fig. 1.

i) a correlation study suggesting variables which are not significantly interrelated and between which interactions may be disregarded,

ii) an orders of magnitude study indicating variables and processes which can be neglected,

iii) a sensitivity analysis evaluating the degree of refinement which is required in the specification of state variables and interaction laws,

iv) a dialogue with the users of the model allowing a more precise definition of the objectives and indicating the degree of sophistication which is required to produce reliable predictions answering the questions put to the model without unnecessary expensive complexity.

2.-

The mathematical model which emerges from the confrontation with the data base is submitted to the scientific reflection.

Data processing, simulation tests and fundamental research contribute to a better understanding of the structure of the system and of the ability of the model to describe it. The assessment of the modelling prospective efficiency combined with specific management requests determines subsets of the general model which can be used for reliable, speedy predictions answering limited purposes and assisting immediate decisions.

The calibration, adjustment and exploitation of the submodels feed back information in the general model whose development, combined with new requests from management objectives, gives birth to second generation submodels with increased reliability.

A continuous interaction between research and application is thus achieved in the guiding framework of mathematical modelling.

To proceed from a general mathematical description to a tractable mathematical model and later to more limited submodels one can :

1) reduce the *support*, *i.e.* the extent of the system in physical space and time either by :
   i) narrowing the field of investigation or
   ii) averaging over one or several space coordinates or over time,

2) reduce the *scope*, *i.e.* the dimensions of the system in state space either by
   i) closing the system at a limited number of state variables (allowing for the global effect of other less essential parameters in adjustable coefficients) or
   ii) averaging over suitably defined compartments of which only the aggregate properties, not the details, are described.

The operating models of the North Sea can all be regarded as reduced size versions of an interdisciplinary three-dimensional model on which one or several simplifications were performed as described above.

i) Integration over depth and reasonable hypotheses on the vertical density distribution have allowed the development of two-dimensional models of tides and storm surges.

ii) Further time integration (over a time sufficiently long to cover several tidal periods and thus cancel to a large extent tidal oscillations and transitory wind currents) has given the residual circulation model where the results of tidal computations are used to calculate the forcing due to non-linear tidal interactions.

iii) Tidal and residual models have been exploited to evaluate the dispersion and the advection of marine constituents and to elaborate dispersion models adapted to the study of coastal discharges of pollutants and off-shore dumpings.

iv) The hydrodynamic models have revealed distinctive marine regions where different current regimes prevail and which appear as natural boxes for the elaboration of completely space integrated time dependent chemical and ecological box models.

Chemical and ecological models have also been simplified by restricting attention to the aggregate properties of compartments such as dissolved substances, suspensions, bottom sediments, phytoplankton, zooplankton, heterotrophic bacteria, fish, ...

The Southern Bight model developed in Belgium demonstrated that in this shallow area of extremely variable depth, the dispersion of pollutants was dominated by the shear effect associated with the vertical variations of very intense tidal currents. The predictions of the size and the shape of patches of pollutants after a release were found in excellent agreement with the observations.

The presence of residual gyres was identified as a major factor in the sedimentation pattern and the existence of ecological niches where distinct ecosystems prevail.

In particular, the gyre discovered off the eastern Belgian coast succeeded in explaining the observed accumulation of mud and heavy metals in the bottom sediments along the coast by the entrainment and prolonged residence of highly turbid waters from the Scheldt estuary.

The model showed that the gyre created, in that region, outer-lagoon conditions characterized by high nutrient concentrations and phytoplankton biomass but little zooplankton grazing and intensive

recycling of nutrients by bacteria (revealing a rather unhealthy short-circuited food chain where additional releases of nutrients might create the conditions of entrophication).

A nutrient cycle box model was elaborated with special emphasis on the coastal gyre region. On that basis, models were derived to simulate the translocation of pollutants (such as heavy metals) from the water column, through the food chain, to the consumable fish. The predicted concentrations in fish were found in good agreement with the measured concentrations in sampled specimens.

Applications and assistance to management

The Southern Bight model can predict with great accuracy the elevation of the water surface produced by tides and storm surges, the dispersion, sedimentation — and eventual recirculation by strong turbulence — of suspended material as well as the final deposition of sediments on the bottom. It can simulate the effect of coastal engineering works (dredging, construction of a harbour, ...) and can give full assistance to management in this respect.

By revealing the existence of distinctive regions where different circulation regimes prevail, the model identified ecological regions which are the natural boxes for adjacent box models describing the dynamics of the Bight's ecosystems. These models can evaluate the fluxes of carbon, nitrogen, ... , pollutants, ... through the food chain and provide an estimate of the anticipated fish population and level of pollution. In this respect the model can assist Public Health decision. Equivalently, it can elaborate on Public Health tolerances to determine acceptable upper bounds for the pollutants' concentrations in coastal waters or sediments.

The model can predict the dispersion pattern of pollutants both in the water column and in the sediments. By evaluating the extent of the dammage produced by a given coastal or off-shore release, the model can thus appreciate the opportunity of authorizing or penalizing dumpings in the sea and assist management decision. Furthermore, determining the transfer functions which relate the intensity of the source (the amount

released) and the final concentrations in the sea, the model, working backwards from Public Health tolerances, can set up for management the problem of optimizing, subject to economical constraints, the tolerable inputs and the locations of sources of pollution, coastal outfalls and sea dumpings.

II.- THE HYDRODYNAMIC SUBMODELS

Based on :
- Math. Modelsea (1974), I.C.E.S. Hydrography Committee, C.M. 1974 - C : 1;
- NIHOUL J.C.J. (1975a), Modelling of Marine Systems, Elsevier Publ., Amsterdam;
- NIHOUL J.C.J. and RONDAY F.C. (1975), Tellus, 27, 5;
- RONDAY F.C. (1975), Ph. D. Dissertation, Liège University.

The models used in this study are depth averaged models which are the most popular (and economical) in shallow barotrophic areas. Let

$$x_3 = - h(x_1, x_2)$$

be the equation of the bottom and

$$x_3 = \zeta(x_1, x_2, t)$$

the equation of the sea surface; the axes $\mathbf{e}_1$ and $\mathbf{e}_2$ pointing to the east and to the north respectively. The transport of water $\mathbf{U}$ integrated over the depth is cleared of turbulent fluctuations whose dispersing effects are taken into account with an "eddy" viscosity. This "eddy" viscosity combines the effects of shear and turbulence [Nihoul (1975a)]. The mean current $\overline{\mathbf{u}}$ over the depth is also often introduced :

$$\mathbf{U} = \overline{\mathbf{u}}\, H = \frac{1}{H} \int_h^{\zeta} \mathbf{u}\, dx_3 \tag{1}$$

where $H = h + \zeta$

is the instantaneous depth.

1.- Tidal and storm surge model (transient state)

1.1.- Equations of motion

The basic equations can be written [*e.g.* Nihoul (1975a)] :

$$\frac{\partial H}{\partial t} + \nabla . \mathbf{U} = 0 \tag{2}$$

$$(3)\quad \frac{\partial U}{\partial t} + \nabla . (H^{-1}\, U\, U) + f\, e_3 \wedge U = H[\xi - \nabla(\frac{p_a}{\rho} + g\, \zeta)] + a\, \nabla^2 U - \frac{D}{H^2} \|U\|\, U + C_{10}\, V\, \|V\|$$

where f is the Coriolis parameter, ξ the astronomical tide producing force per unit mass, p_a the atmospheric pressure, a the appropriate "eddy" viscosity, V the wind speed at the anemometer level (10 meters), C_{10} the experimental drag coefficient at the sea surface and D the bottom friction coefficient.

The order of magnitude of the shear effect viscosity is $a_{sh} \sim 50\ m^2/s$. Nihoul (1975a) shows that the turbulent contribution is weak. For long waves the diffusive term can be easily estimated : in the most irregular part of the North Sea

$$a\, \frac{\partial^2 U}{\partial x_1^2} \sim 50 . \frac{10}{(2\ 10^4)^2} \sim 10^{-6}\ m^2.s^{-2} .$$

This term is thus much smaller than the Coriolis, pressure and inertial terms (10^{-3} to $10^{-4}\ m^2.s^{-2}$) and will be neglected in the models.

1.2.- Boundary conditions

The North Sea is limited by coasts and by open sea boundaries; two kinds of conditions must be used :

i) along the coast

One assumes

$$\frac{\partial U}{\partial n} = 0$$

where n is the normal unit vector pointing outward. For a zonal coast one imposes $U_2 = 0$, and for a meridian coast $U_1 = 0$.

ii) along an open sea boundary

Equations for long waves are hyperbolic, one must impose either the sea level or the water transport along an open sea boundary. This information is supplied by experiments or by numerical predictions from other models characterized by coarser grids.

1.2.1.- For the Strait of Dover

It is difficult to have experimental current data in the Straits of Dover. Moreover the current is very sensitive to variations of the depth. For these reasons sea level data are used as boundary conditions. A linear interpolation for the sea level can provide good conditions across the Straits.

1.2.2.- For the Skagerrak

From numerical experiments the tidal influence of the Skagerrak on the North Sea system is weak. Small errors in the estimation of the sea level across this open sea boundary will not perturbe too much the whole area.

1.2.3.- For the North Atlantic Entrance

The bathymetry near the 60th parallel is characterized by a large plateau with a mean depth of 180 meters and by a deep channel of 400 meters. Along this open sea boundary amplitude and phase of tides and storm surges are known only at coastal stations (The Liverpool Tidal Institute uses now pressure gauges along the continental shelf; but these data are not yet available).

i) for tidal waves

Taylor (1922) and Godin (1966) studied the propagation of tides in rectangular bays. They found that far from the reflection area the wave has the character of a Kelvin wave. The behaviour of the tidal wave in the northern part of the North Sea is thus similar to a Kelvin wave. In this model one assumes a constant phase for the tide along a line perpendicular to the British coast.

To calculate the phase along the open sea boundary *for the plateau* the following relation is used *for the M_2 tide*

$$\phi_r = \phi_{ref} \pm \frac{r}{\sqrt{gh}} \frac{360}{T_{M_2}} \text{ in degrees ,}$$

where T_{M_2} is the period of the M_2 tide, r the distance between the open sea boundary and the reference phase line, + r if the open sea

boundary line is below the reference line, $-r$ if the open sea boundary line is above the reference line. ϕ_{ref} is the phase at a tidal coastal station. This formula gives us the value of ϕ at the Norwegian Trench. A linear interpolation between ϕ_{NT} and the phase at the Norwegian tidal coastal station is used across the Norwegian Channel.

As the tidal wave has the character of a Kelvin wave at the Northern entrance the amplitude profile of the sea elevation is assumed exponential : only one boundary condition is required to define it completely. At the west side, the amplitude is approximately equal to 1.2 m , the Kelvin wave profile gives an amplitude at the Norwegian Trench $A \sim 0.48$ m ; at the east side of the boundary, the amplitude is 0.4 m and the Kelvin wave profile gives also 0.48 m at the separation "point" between the plateau and the Norwegian Channel. One can thus assume a Kelvin profile for the tidal waves.

ii) storm surges

The estimation of the cross profile of the sea level for a storm surge is very difficult. Until results from data pressure sensors are available, one makes a linear interpolation between coastal stations.

2.- Residual circulation model

2.1.- Equations of the model

The mean flow U_0 is obtained from the time-averaged equations [*e.g.* Nihoul (1975a), Nihoul and Ronday (1975)] :

$$f\, e_3 \wedge U_0 = - H_0\, \nabla\left(\frac{p_a}{\rho} + g\, \zeta_0\right) - K\, H_0^{-1}\, U_0 + \Theta_0 \qquad (4)$$

where $K = D\, \| \overline{u}_1 \|_0$

is the new friction coefficient and is function of the amplitude of the non stationary current field. For the North Sea $\overline{u}_1$ is of the order of 1 m/s in the average; thus

$$K \sim D\, \| \overline{u} \|_0 \sim 2\ 10^{-3} \text{ m/s} .$$

$$\Theta_0 = \tau_w + \tau_t$$

is the new stress which combines the average wind stress

$$\tau_w = (C_{10}\, V \,\|V\|)_0$$

and the "tidal stress" calculated by averaging the non stationary equations

$$\tau_t = - [g\, \zeta_1\, \nabla\zeta_1 + \nabla . (H^{-1}\, U\, U)]_0 \tag{5}$$

For the residual circulation the geostrophic wind is calculated by means of atmospheric pressure data. The surface wind is derived from the geostrophic wind by classical empirical formulas. The mean surface stress over a period of one year is equal to

$$\tau_w = 0.2\ 10^{-4}\ m^2/s^2 \ .$$

The continuity equation for the mean flow allows the definition of a stream function ψ

$$U_{0,1} = - \frac{\partial \psi}{\partial x_2} \qquad\qquad U_{0,2} = \frac{\partial \psi}{\partial x_1} \tag{6}$$

Dividing equation (4) by H_0 and taking the curl in order to eliminate the surface elevation, one obtains :

$$K\, \nabla^2 \psi - \frac{\partial \psi}{\partial x_1} \left(f \frac{\partial H_0}{\partial x_2} + \frac{2K}{H_0} \frac{\partial H_0}{\partial x_1} - \beta \right) + \frac{\partial \psi}{\partial x_2} \left(f \frac{\partial H_0}{\partial x_1} - \frac{2K}{H_0} \frac{\partial H_0}{\partial x_2} \right)$$

$$= H_0\, \omega_3 + \frac{\partial H_0}{\partial x_2}\, \Theta_1 - \frac{\partial H_0}{\partial x_1}\, \Theta_2 \tag{7}$$

where $\omega_3 = (\nabla \wedge \Theta_0)_3$

$\beta = \frac{df}{dy}$ is the beta factor introduced by Rossby in order to take into account the variability of the Coriolis term with the latitude.

The stream function ψ can be split in three parts :

$$\psi = \psi_{stress} + \psi_{interaction} + \psi_{leak}$$

ψ_{stress} induces a circulation directly related to the stress Θ ;
$\psi_{interaction}$ creates a circulation which depends on the gradient of the depth; ψ_{leak} gives the contribution of exterior flows to the model.

2.2.- Boundary conditions

The North Sea is limited by coasts and by open sea boundaries. Two kinds of conditions must be used.

i) along coasts

One assumes that the water transport across the coast is zero. The stream function ψ is then a constant along a coast.

ii) along open sea boundaries

Estimates of water fluxes across open sea boundaries

The inflow of water from the North Atlantic is estimated at 23000 km^3/year [Kalle (1949)]. For the flow through the Straits of Dover Cartwright's (1961) figures give 7400 km^3/year . This value is many times higher than the former estimates [Carruthers (1935)], but this value is now accepted as being nearly correct. Wyrtki (1954) showed that the water balance of the Baltic Sea is complicated. Over short periods of time different authors have found either an outflow or an inflow according to atmospheric conditions. In view of these complexities, the figures of 200 km^3/year given by Leavastu (1963) for a long period of observation seem to provide a reasonable guide to the long-term mean inflow. Due to the lack of precise long-term measurements across the Skagerrak one imposes a stream function at the two sides of the channel with a difference proportional to the net inflow. Inside this open sea boundary it is assumed that the current is unidirectional : in this model this condition implies $\frac{\partial \psi}{\partial n} = 0$ where n is the normal to the boundary.

The most important rivers are the Meuse, the Rhine and the Scheldt which provide a new inflow of 63 km^3/y . The other inputs come from German estuaries (60 km^3/y) and from S.W. Norway. If one assumes that rain (inflow) is balanced by evaporation (outflow) and a steady state water budget, one obtains 30789 km^3/y for the water outflow in the North Atlantic. Observations reveal that the outflow is mainly concentrated in the region of the Trench. In this model one imposes an inflow between the Scottish coast and the third east meridian and an outflow from that meridian to the Norwegian coast. In these two sections a uniform distribution of the flow is assumed.

3.- Results of computations

The procedure of computations for the transient and residual circulation is given on the following flow chart :

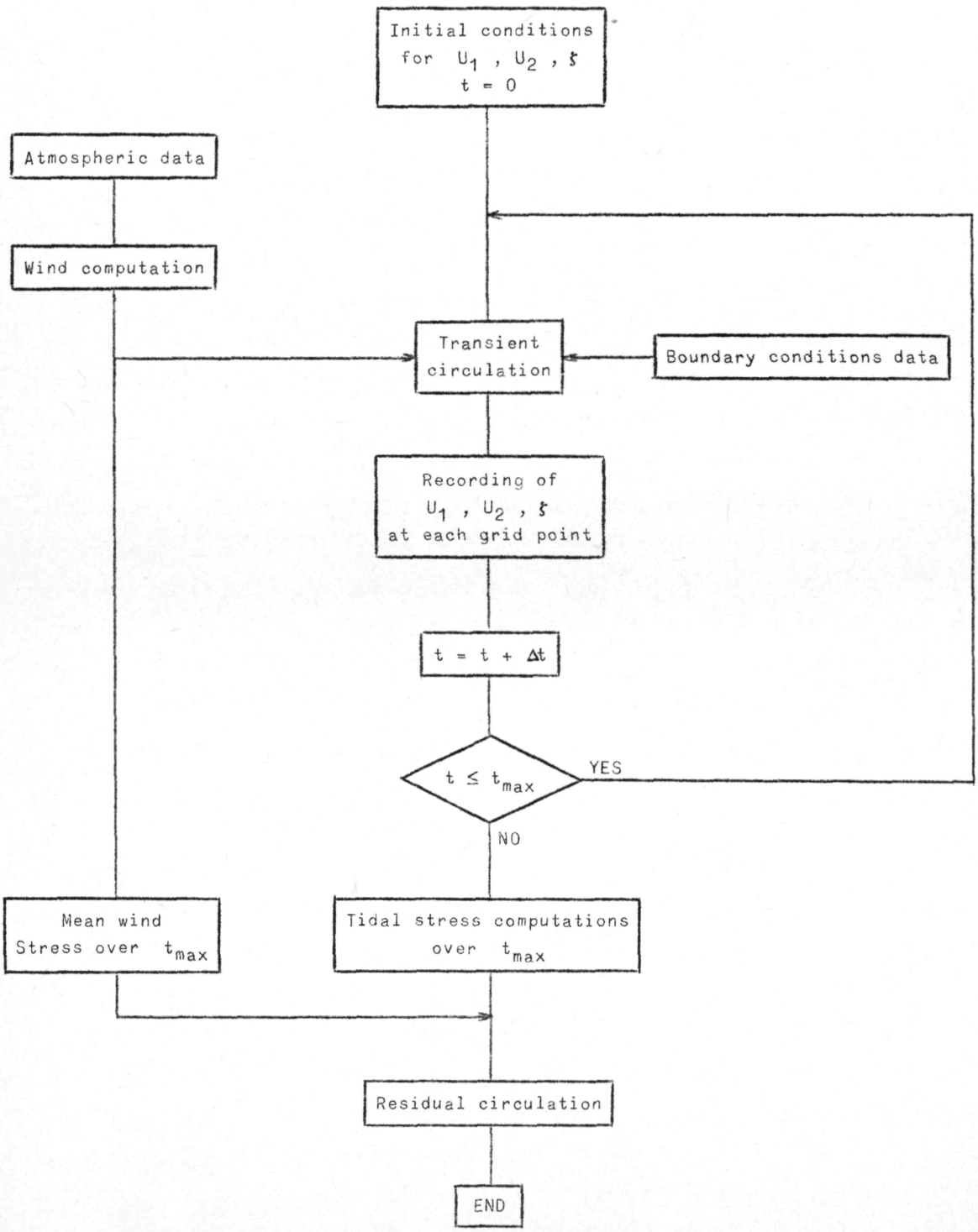

The equations for the residual circulation are solved by classical methods.

3.1.- Transient circulation

The current regime in the North Sea is mostly tidal. The most important partial tide is the lunar semi-diurnal. Coastal tidal data are well known and come from the *Table des constantes harmoniques de Monaco*.

Currents and sea elevations are not purely harmonical function of time due to non linear terms in the equations of motion. These non linearities appear in shallow areas : the Belgian, Dutch, German, Danish coast are characterized by shallow waters. In order to compare the amplitude and phase of the M_2 tide at coastal stations, a Fourier analysis of the sea-level is carried out. The comparison between observed and calculated amplitudes and phases for coastal stations shows a very good agreement. Some discrepancies appear along the British coast for the amplitude due to very sharp depth variations. Near Lowestoft (Suffolk) some differences exist for the phase of the tide because this region is submitted to the influences of the North Atlantic and Dover Strait tidal forces. A slight error in the estimation of sea levels along open sea boundaries strongly modifies the phase of the tide in these regions. The approximation of the coastline by a rectangular grid introduces also errors : the wave phase is thus very sensitive to the position of the numerical grid.

Cotidal and corange lines are given in figures 2 and 3. The agreement is good. Due to the small number and low quality of sea level measurements in the inner part of the North Sea one can conclude that the present model gives better results than those provided by Proudman and Doodson (1924).

Tidal currents measured and calculated are also compared; the agreement is very satisfactory. Measurements should be concentrated along the open sea boundaries with some measurements in the central part of the grid to verify the quality of the model. Results from computations agree with measurements (the error is of the order of the experimental

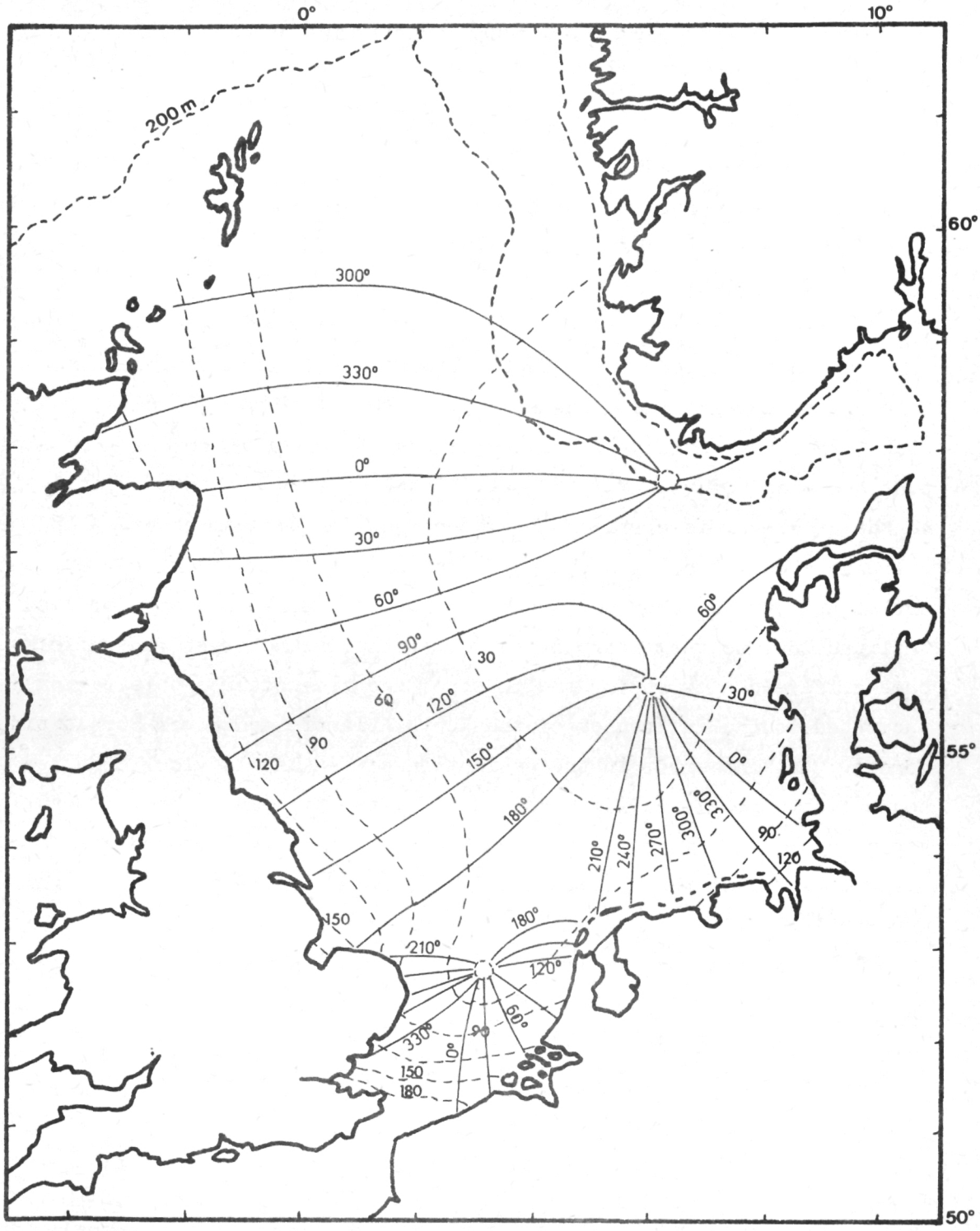

fig. 2.

Lines of equal tidal phases and amplitudes in the North Sea according to the mathematical model.

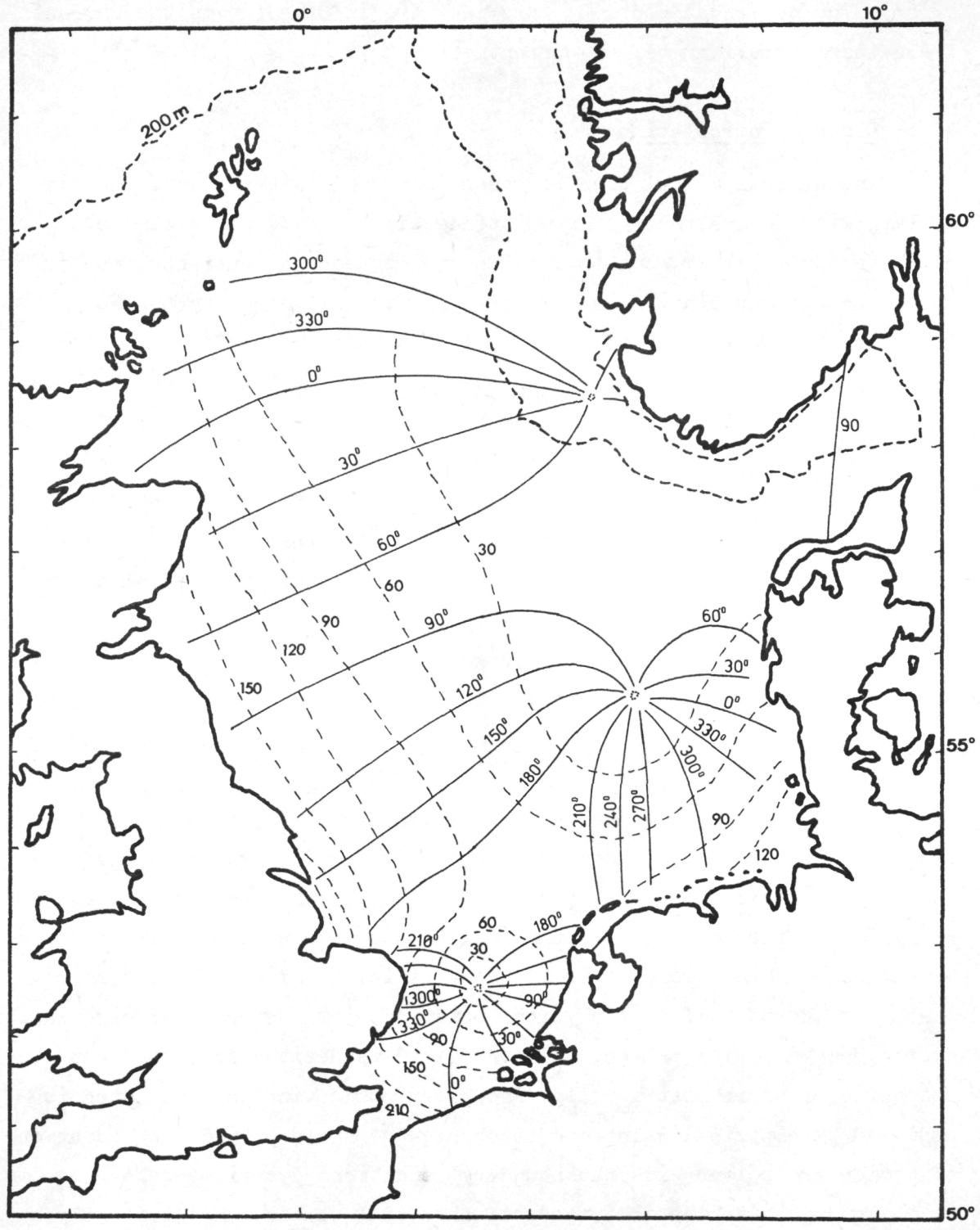

fig. 3.

Lines of equal tidal phases and amplitudes in the North Sea according to observations (after Proudman and Doodson, 1924).

error). The numerical model can provide more information on the current field than a small number of currentmeter stations.

3.2.- Residual circulation

The general circulation in oceans is mostly wind-driven. One can explain with such a theory the existence of the different well-known currents (Gulf Stream, Equatorial, Counter-equatorial currents, etc.). The long-term circulation in the North Sea is influenced by the North Atlantic current which enters the North Sea through the Straits of Dover and through the Channel between the Orcades and Shetland Isles. The influence of the Baltic sea is weak but provides water with a low content of salt (< 34 ‰). From oceanographic measurements (T , S , O_2) it is possible to determine the general distribution of the different water masses [Böhnecke (1922), Laevastu (1963)] (see figure 4).

In winter the North Sea water has no haline and no thermal stratifications except in the Norwegian Channel and near the coast line. The barotropic model can be used. In summer the haline stratification remains weak but a thermal stratification exists in the northern and central part of the bassin. The barotropic model may give approximate results during that period of time.

One assumes here that the water is vertically homogeneous, and a barotropic model is used. Böhnecke (1922) and Laevastu (1963) observed that the circulation pattern remained unchanged all around the year. The difference between summer and winter circulations is determined by the size of the areas of influence (spatial modification of vortex).

To understand from a physical point of view the residual circulation over a one-year time period, the wind field is derived from the mean atmospheric pressure distribution. The geostrophic wind so calculated is modified by empirical relations to obtain the surface wind. The equations of motion are solved with the boundary conditions described before.

To emphasize the importance of the tidal stress, one first solves the equations for the residual circulation without explicitly taking the tidal stress into account (figure 5). The wide stream coming from the North Channel flows down the British coast as far as East Anglia. The

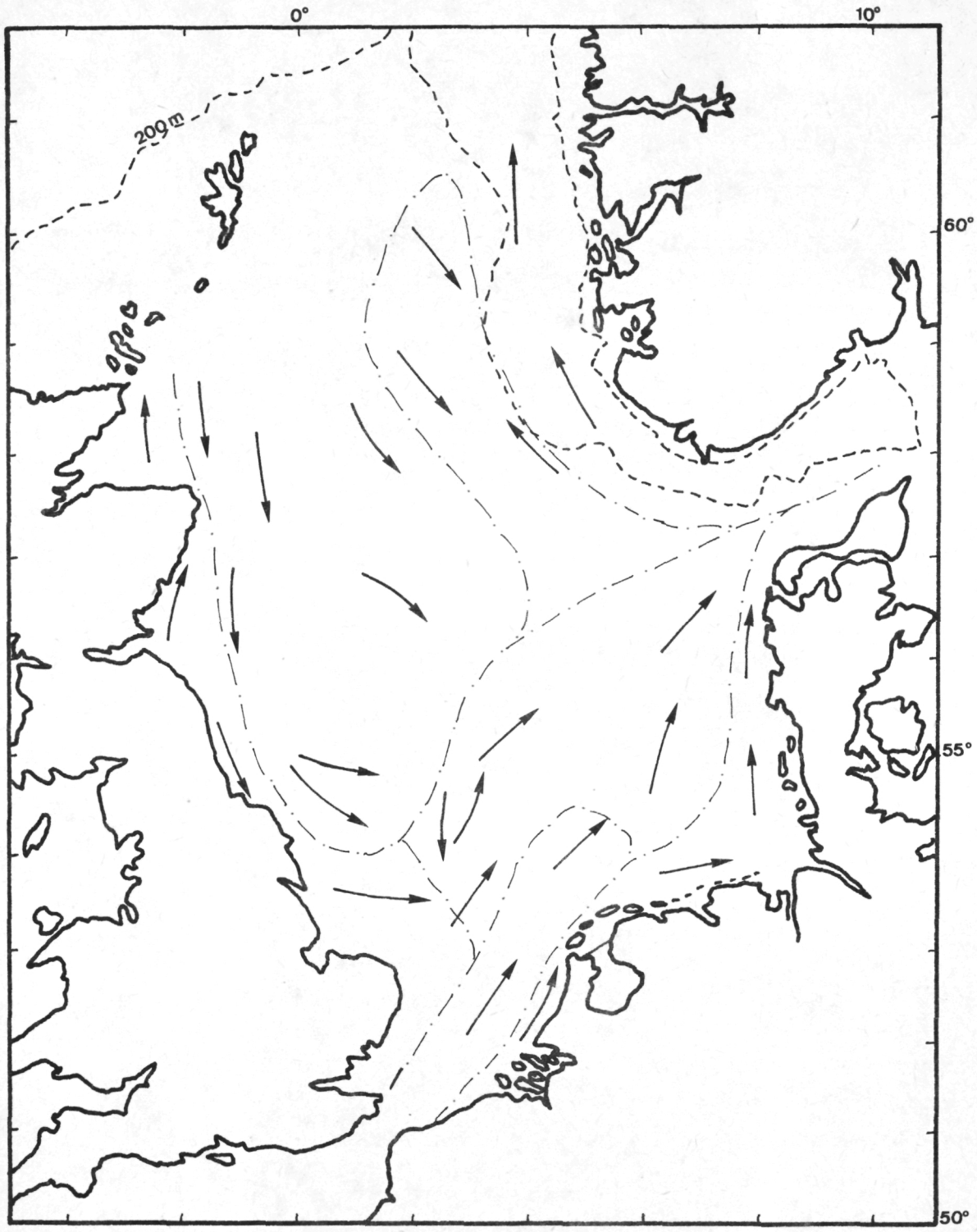

fig. 4.
Water masses in the North Sea according to Laevastu (1963).

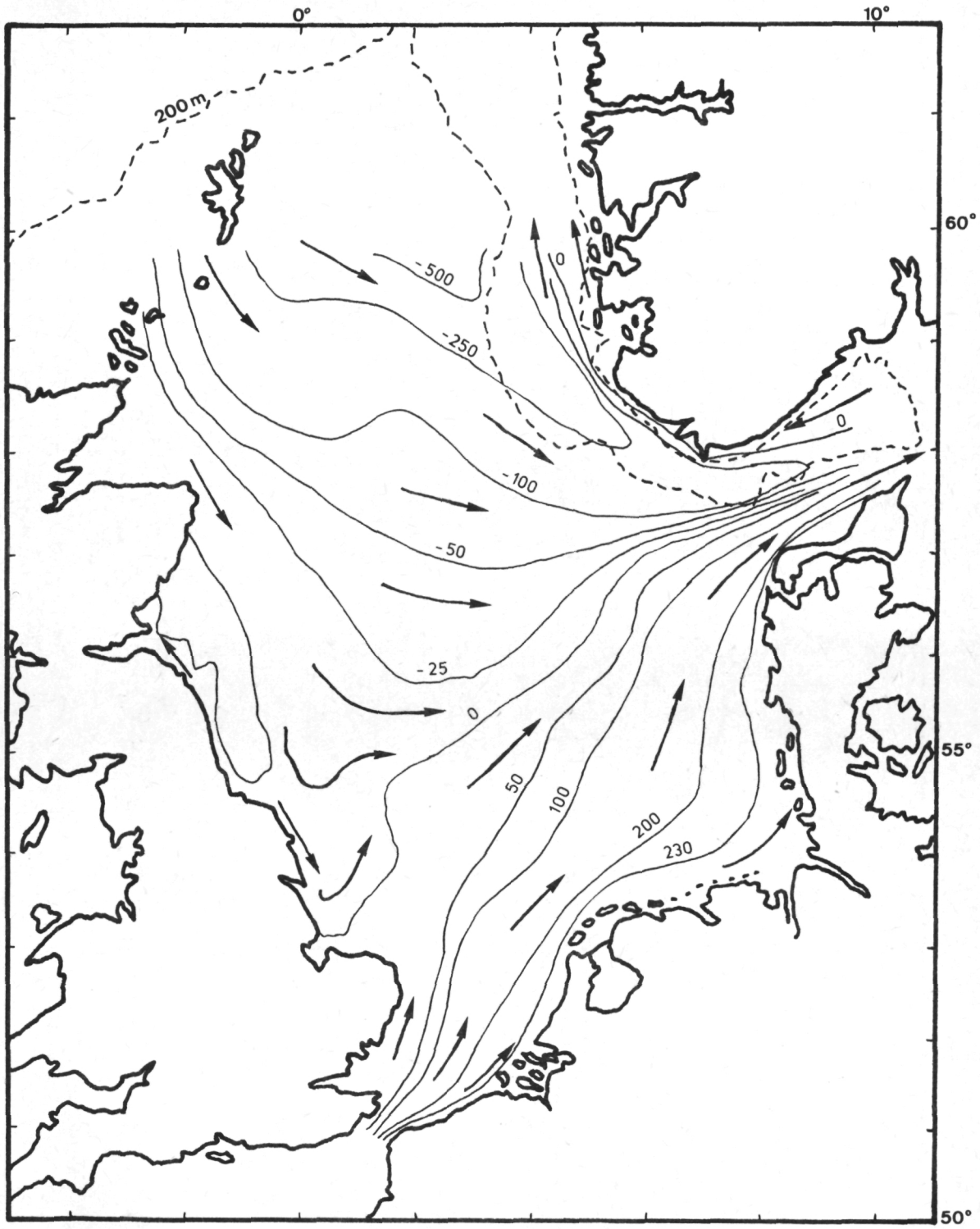

fig. 5.
Residual circulation calculated without tidal stress.
ψ = const (in 10^3 m^3/s)

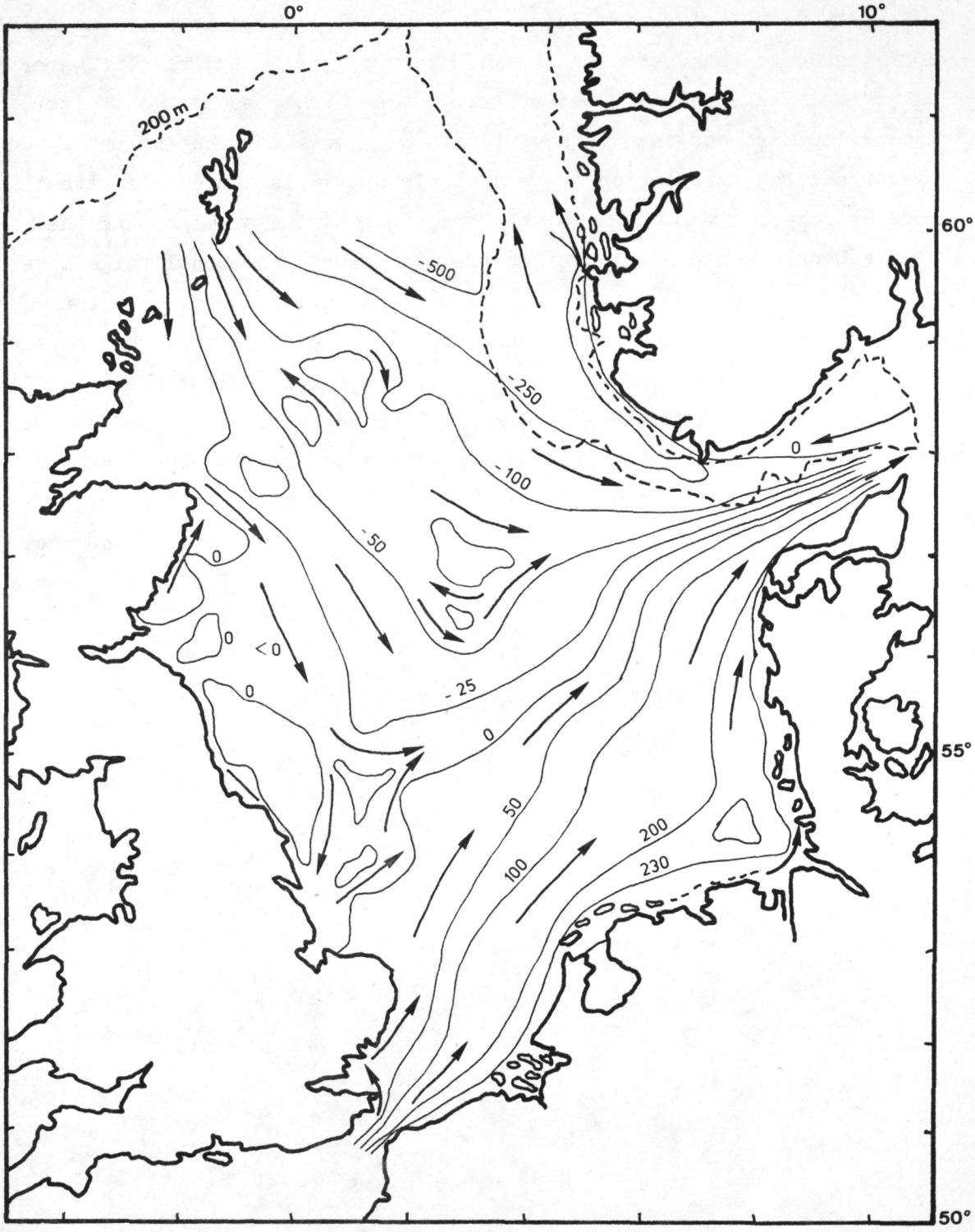

fig. 6.
Residual circulation calculated with the tidal stress.
ψ = const (in 10^3 m^3/s)

intensity of the stream is decreasing southerly; there is only one swirl near the Scottish coast line. A small part of the North Atlantic water enters the Skagerrak. The Dover Strait stream is broadening out after some kilometers and the width of this stream remains constant until the Skagerrak. The circulation is very simple but it is impossible with this model to explain the swirl in the German Bight, the swirl around the Dogger Bank and the swirl near the Belgian coast. The model which takes into account the tidal stress is the only one able to reproduce the actual residual circulation (figure 6). The general pattern remains but important modifications appear in different regions. Along the British coast and in the German Bight swirls exist and are observed for a long time [*e.g.* Hill (1973)]. Figure 6 exhibits also another vortex around the Dogger Bank; Ramster (1965) proves its existence with sea-bed drifters. Other swirls exist in the central part of the North Sea where the residual current was very weak in the former model (figure 5). The model reveals also a south westerly current near the Belgian coast.

III.- MUD DEPOSITION IN THE SOUTHERN BIGHT

Based on :

- Math. Modelsea (1974), I.C.E.S. Hydrography Committee, C.M. 1974 - C : 1;
- NIHOUL J.C.J. (1975c), Effect of the tidal stress on mud deposition in the Southern Bight of the North Sea, Proc. 2d Annual Meeting of the European Geophysical Society, Trieste 20-26 Sept. 1974.

During 1972 and 1973, some 1200 samples were analysed, taken at regular intervals, mostly with a Van Veen sampler, in the Southern Bight of the North Sea. As described by Gullentops (1974) : "The Southern Bight is strikingly free of muddy sediments, indicating that currents and here also wave turbulence are high enough to allow only temporary decantation but no final deposition. Only in front of the Meuse-Rhine mouth, increased fluvial input of suspension material influences the bottom sediments. The big exception is the low energy triangle in front of the eastern Belgian coast in which muddy sedimentation is developing to a considerable extent due to local affluents as the Yser, but mostly to the suspension material dragged out of the Scheldt estuary and trapped in this area.

"ERTS-A remote sensing documents proved this fact strikingly, showing a suspension plume in front of the Rhine mouth and a huge turbid area in front of the eastern Belgian coast connected with an extremely turbid Scheldt estuary.

"The mud area could *in globo* be explained by the tendency to form an outerlagoon, behind the prelittoral ridges, in which increased suspended matter arrival tends to be preserved by the current pattern, is flocculated and aggregated by biological activity and preserved from net erosion by weakened wave activity."

The observations [Elskens (1974)] show the eastern Belgian coast to be a privileged zone of mud accumulation in relation to the whole network studied.

Figure 7 [Nihoul (1975a)] shows the residual currents pattern derived from the simple classical model in which the Reynolds stress, the shear

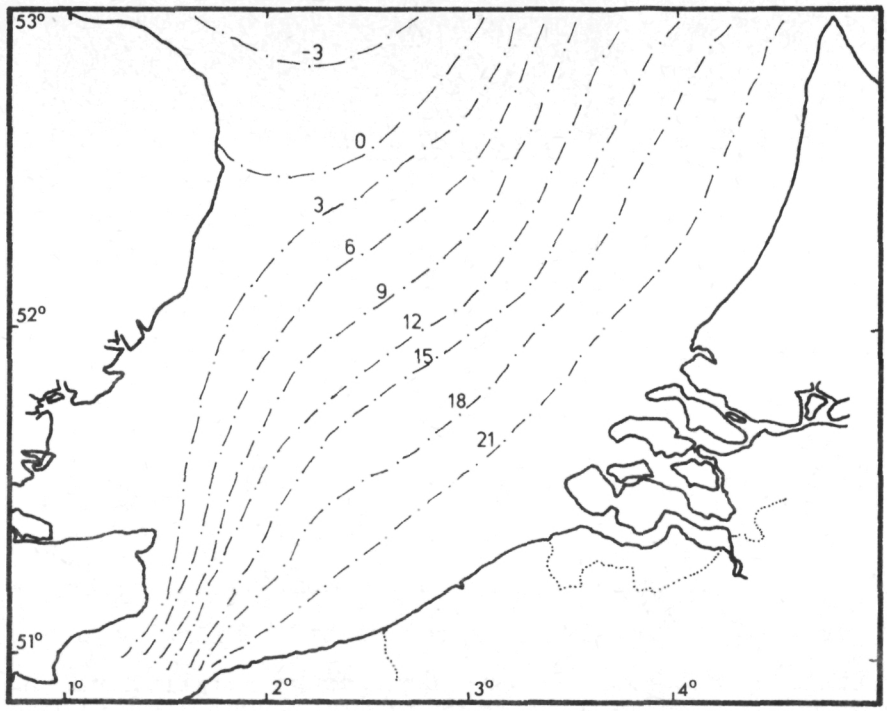

fig. 7.
Residual circulation in the Southern Bight without tidal stress.
Streamlines ψ = const (in 10^4 m^3/s)

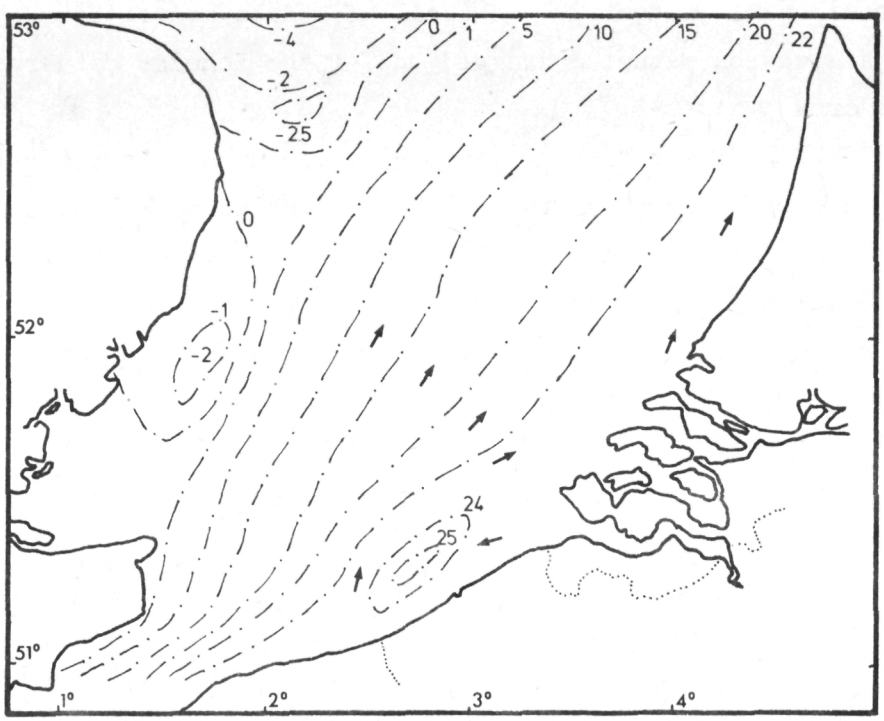

fig. 8.
Residual circulation in the Southern Bight with the tidal stress.
Streamlines ψ = const (in 10^4 m^3/s)

stress *and* the tidal stress are approximated by a diffusion term. Such a pattern – although it reproduces the expected North bound flow from the Straits of Dover – cannot explain the observations of deposited sediments.

On the contrary, the new model described in section II predicts the existence of a residual gyre off the Belgian coast which, increasing the residence time of the water masses and in particular the entrained water from the Scheldt estuary, fully explains the observed sedimentation pattern (figure 8).

IV.- ECOSYSTEMS DYNAMICS IN THE SOUTHERN BIGHT

Based on :

- Math. Modelsea (1974), I.C.E.S. Hydrography Committee, C.M. 1974 - C : 1;
- NIHOUL J.C.J. (1975d), Mesoscale secondary flows. Implications in the chemical and biochemical dynamics of the Southern Bight, Proc. Liège 6th Colloquium on Ocean Hydrodynamics, Liège, April 28 - May 2, 1974.

An extensive survey of chemical and ecological variables in the eastern part of the Southern Bight was made during the years 1971, 1972, 1973 and 1974 in the scope of the Belgian National Program on the Environment, Sea Project. On the basis of these informations, the survey region was divided into three zones where different conditions prevail (figure 9).

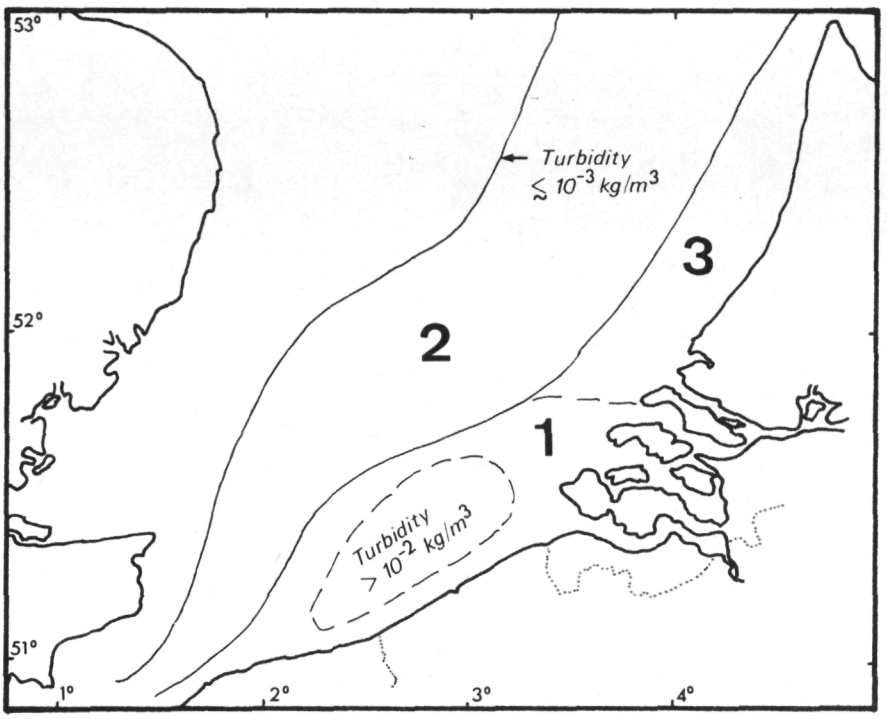

fig. 9.

Three zones in the Southern Bight where a different pattern of residual circulation is predicted by the model and which also appear from the observations as three distinct boxes.

One can see that the different zones correspond to different residual circulation regimes.

i) Zone 1, off the Belgian coast corresponds to the residual gyre. Water from the Scheldt estuary is to a large extent entrained in the gyre before it can escape to the north. An island of high turbidity ($> 10^{-2}$ kg m^{-3}) is observed in the region where closed stream lines are predicted by the model. Bottom sediments in zone 1 are characterized by large areas of mud which can be explained by the tendency to form — as shown by the residual current model — an outerlagoon "in which increased suspended matter arrival tends to be preserved by the current pattern, is flocculated and aggregated by biological activity and preserved from net erosion by weakened wave activity" [Math. Modelsea (1974)].

ii) Zone 2 corresponds to fairly parallel stream lines showing off the north-bound flow of the branch of the Gulf Stream which penetrates the North Sea through the Straits of Dover. The turbidity in zone 2 is considerably lower and no systematic silt deposition occurs.

iii) Zone 3 corresponds to water masses under direct influence of the Meuse-Rhine estuary. The rivers' outfall is in a sense prolonged into the Sea by a residual flow parallel to the Dutch coast, to the north.

The lagoon conditions which result from the residual circulation in zone 1 is responsible for striking differences between the dynamics of the ecosystems in that region and in zone 2.

The high turbidity of the water in zone 1 causes light extinction and reduces primary productivity. The dominance of microplankton in that region (as compared to nannoplankton in zone 2) with a higher half saturation constant could affect productivity in the same way. Taking into account, also, that the depth is smaller in the coastal region, one should expect the integrated production (over depth) to be considerably smaller in zone 1. Observations reveal however that — although there are differences in the annual variations — the yearly average is about the same in the two regions [Podamo (1974)].

This result is obviously related to the much higher nutrient concentration and the much larger specific phytoplankton biomass (measured

by chlorophyll a) observed in zone 1 where lagoon conditions prevail [Podamo (1974)].

Additional information is provided by the ratio phaeophytin a/ chlorophyll a which is systematically larger than one in zone 1 and smaller than one in zone 2; indicating that, in zone 1, most of the phytoplankton cells are dead cells. Zooplankton grazing, on the other hand, is more important in zone 2 than in zone 1, where planktonic and benthic heterotrophic bacteria seem to play the essential role.

A picture thus emerges of a fairly well balanced ecosystem in zone 2 and a rather unhealthy one in zone 1 where intensive phytoplankton production occurs but not, as it should, to provide first level food in the food chain. The phytoplankton crop is harvested only to a small extent. Most of it is left to rot and most of the recycling of nutrients occurs at the dead phytoplankton level under the action of bacteria.

The dynamics of the ecosystems thus reflects the residual circulation patterns and the outerlagoon situation created by the residual gyre in zone 1.

V.- *DISPERSION AND SEDIMENTATION AROUND A DUMPING GROUND*

Based on :

- NIHOUL J.C.J. (1974), Diffusion of turbidity by shear effect and turbulence in the Southern Bight of the North Sea, Proc. Symp. on Turbulent Diffusion in Environmental Pollution, Charlottesville, April 8-14 1973, Advances in Geophysics, 18 A, 331;
- NIHOUL J.C.J. (1975a), Modelling of Marine Systems, Elsevier Publ., Amsterdam;
- NIHOUL J.C.J. and ADAM Y. (1974), Programme national sur l'environnement physique et biologique, C.I.P.S., N 36.

Dumpings in the sea — even though the dumped material may not be toxic as such — create, in many cases, an important pollution problem associated with the local increase of turbidity and the deposition of sediments on the bottom. Solid particles in suspension affect the transparency of the water and may reduce photosynthesis. Silt deposits on the other hand may affect benthic communities and may be in shallow areas prejudiciable to eggs and larvae.

In shallow seas, one is particularly interested in the mean sediments concentration in the water column and in the concentration of bottom sediments.

The equation describing the evolution of the mean concentration of suspensions is derived from the three-dimensional dispersion equation by integration over depth. The average over depth of the quadratic advection terms gives two contributions; the first one contains the product of the means, the second one the mean product of the deviations around the means.

The structure of the latter is analogous to that of the Reynolds stress and experiments reveal that it is indeed responsible for an enhanced dispersion comparable to — but often more important than — the turbulent dispersion. This effect is called the "shear effect" because it is associated with the existence of a vertical velocity gradient.

The shear effect has been described by several authors in pipes, channels and estuaries where, after integration over the cross section, the flow — steady or oscillating — is essentially in one direction [Taylor (1953), (1954); Elder (1959); Bowden (1965)].

In the shallow waters of the Southern Bight, it is generally sufficient to consider the mean concentrations over the depth but, out at sea, no further averaging is possible and the dispersion mechanism is fundamentally two-dimensional. A generalized model was thus developed to account for the rotation of the tidal velocity vector and also include the sedimentation and partial recirculation of the solid suspensions [Nihoul (1974), (1975)].

If $\bar{c}$ and C denote respectively the mean specific mass of suspensions (the depth-averaged mass of suspensions per unit volume) and the specific mass of bottom deposits (the mass of deposited sediments per unit bottom surface) the equations governing the evolution of $\bar{c}$ and C following a dumping at sea can be written [Nihoul and Adam (1974)] :

$$\frac{\partial \bar{c}}{\partial t} + \bar{\mathbf{u}} \cdot \nabla \bar{c} = H^{-1} \nabla \cdot H[\gamma \frac{H}{\bar{\bar{u}}} \bar{\mathbf{u}}(\bar{\mathbf{u}} \cdot \nabla \bar{c})] - H^{-1} \bar{c} \sigma (1 - \frac{\bar{u}^2}{u_c^2}) + \nabla \cdot (\nu \nabla \bar{c}) \tag{8}$$

$$\frac{\partial C}{\partial t} = \bar{c} \sigma (1 - \frac{\bar{u}^2}{u_c^2}) \tag{9}$$

where $\bar{\mathbf{u}}$ is the depth averaged advection velocity, H is the total depth, γ the shear effect coefficient, σ the sedimentation velocity, ν the turbulent diffusivity and where u_c denotes the critical value of $\bar{u}$ above which disruption of the bottom layer by turbulence reverses the sedimentation flux and recirculates sediments in the water column.

It can be shown that the expression for the sedimentation-erosion flux is a first approximation valid for mean velocities $\bar{u}$ never too large compared to the critical value u_c . For larger values of the ratio $\frac{\bar{u}}{u_c}$ more sophisticated formulas must be used and in particular one must take into account that the velocity $\bar{u}$ may exceed a second critical value u_e for which erosion of consolidated bottom sediments may occur. This problem is discussed in the next section.

Knowing the currents and the surface elevations ζ (from atlases or hydrodynamic models), knowing the depth h and thus the total depth

$H = h + \zeta$, the sedimentation velocity of the dumped particles, the turbulent diffusivity and the critical velocity u_c , one can solve equations (8) and (9) and predict as a function of time the evolutions of the patch of suspensions and of the bottom deposits.

Off the Belgian coasts, several dumpings take place periodically in the vicinity of 51° 30' N ; 3° E . These dumpings have been simulated on IBM 370-58 to evaluate their effect on the water turbidity and the deposition of sediments.

The tidal currents which dominate in the area are determined by numerical models and atlases of coastal currents. The critical velocity is estimated at $u_c \sim 0.8$ m/s and is exceeded during a fraction of the tidal cycle. The shear effect coefficient calculated using the vertical velocity profile valid in that region is found to be $\gamma \sim 0.45$. The sedimentation velocity is taken for the particular example chosen as $\sigma \sim 10^{-3}$ m/s .

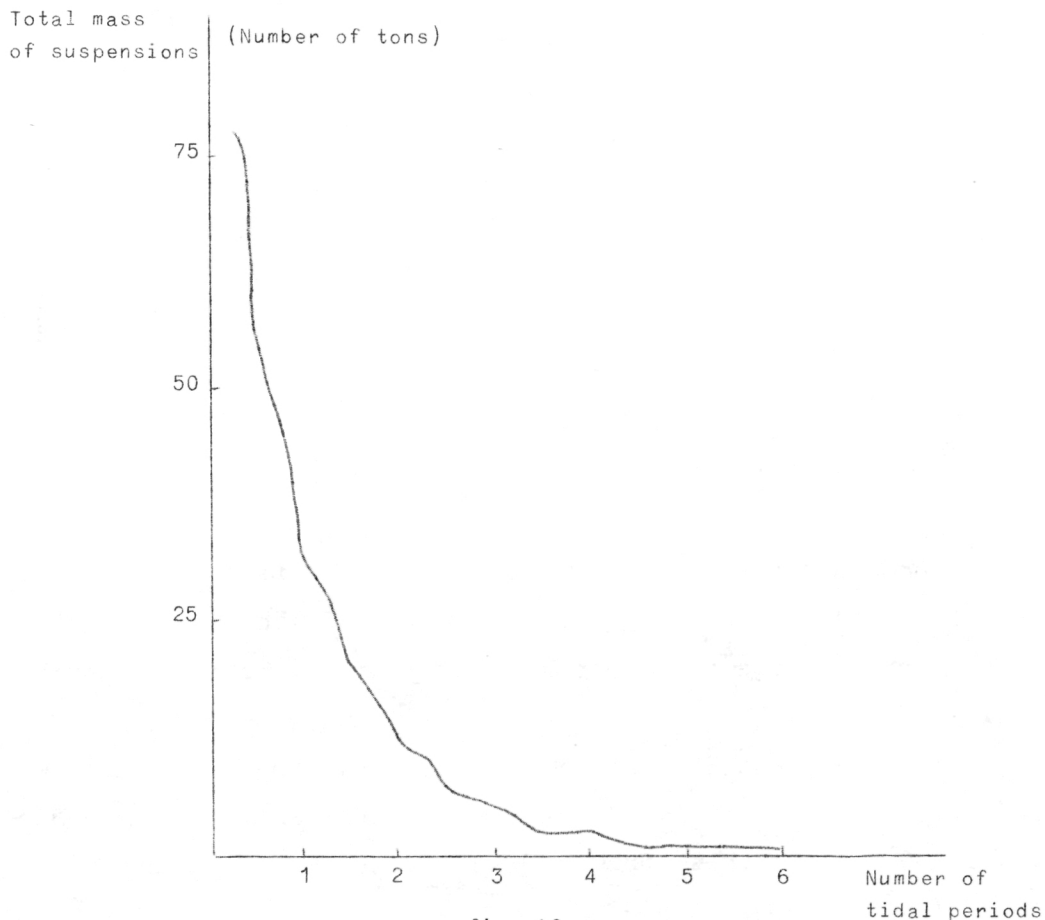

fig. 10.

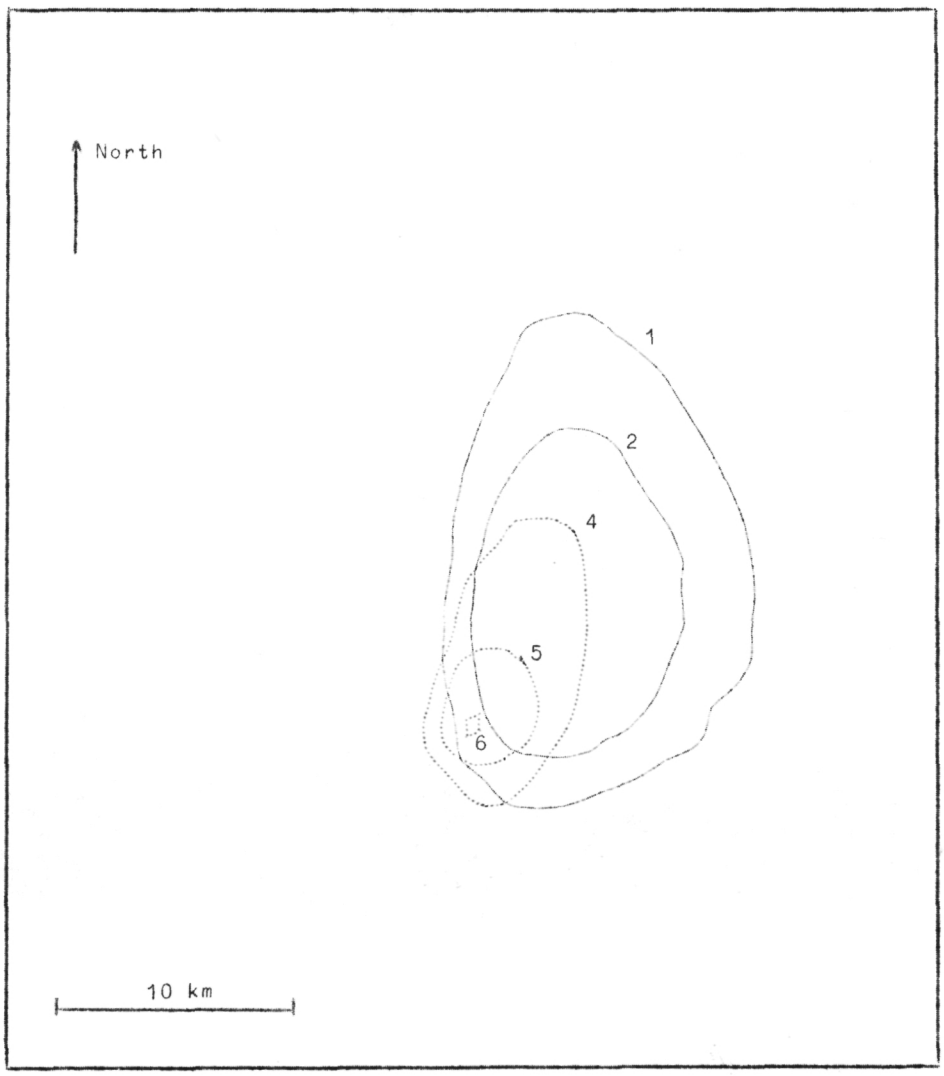

fig. 11.
Isoconcentrations $\frac{1}{4}$ tidal period after the release.

Figure 10 shows the evolution with time of the total mass of suspensions in the water column. Figures 11 and 12 show the evolution over a tidal period of the curves of equal concentrations of suspensions and deposits.

Curves 1, 2 and 3 correspond respectively to concentrations of 1 mg/m^3 , 10 mg/m^3 and 100 mg/m^3 of suspensions. (No curve 3 can actually be seen on these figures because such high concentrations only

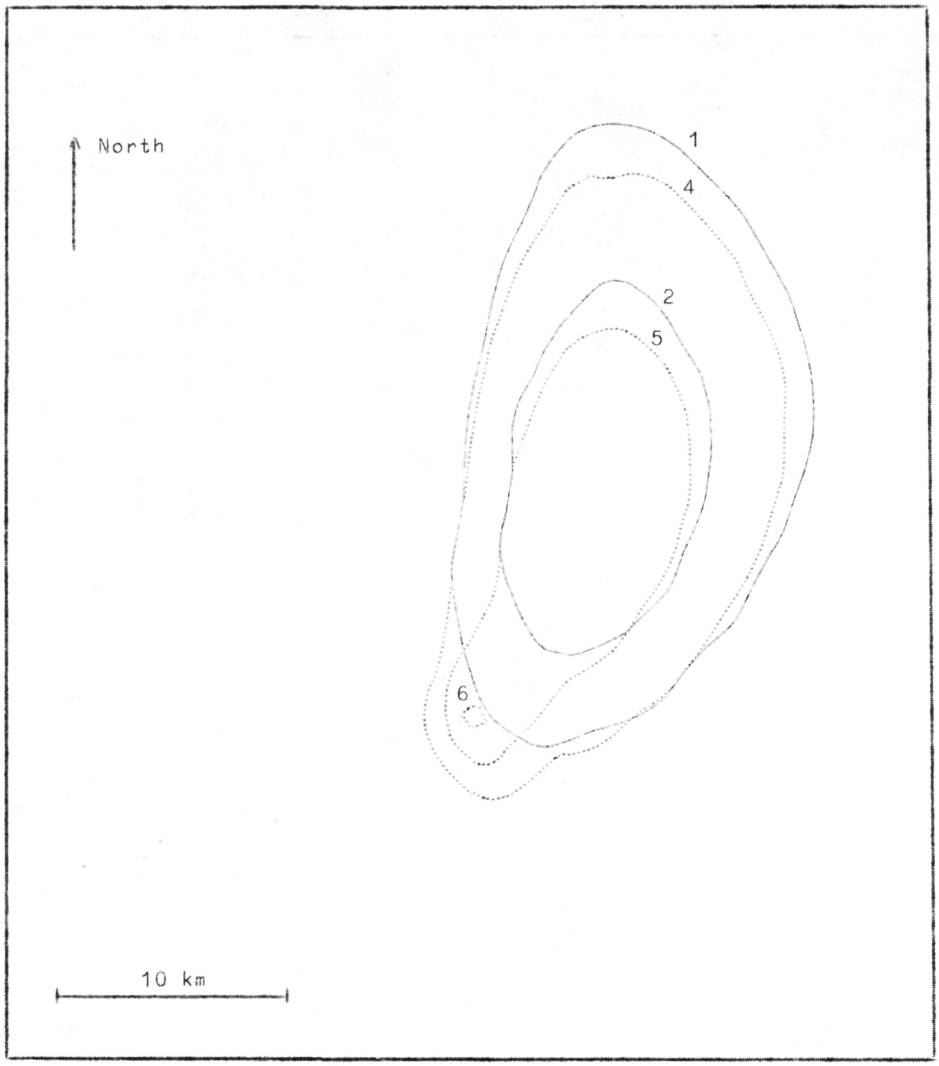

fig. 12.
Isoconcentrations $\frac{1}{2}$ tidal period after the release.

appear around the point of dumping in the first few hours following it and are no longer visible after a quarter of the tidal period.)

Curves 4, 5 and 6 correspond respectively to concentrations of 10 mg/m^2 , 100 mg/m^2 and 500 mg/m^2 of deposited sediments. (Curve 6 or its southern part on figures 13 and 14 may be regarded as locating the dumping ground.)

The results of the numerical simulation are in excellent agreement with the observations. The essential points are :

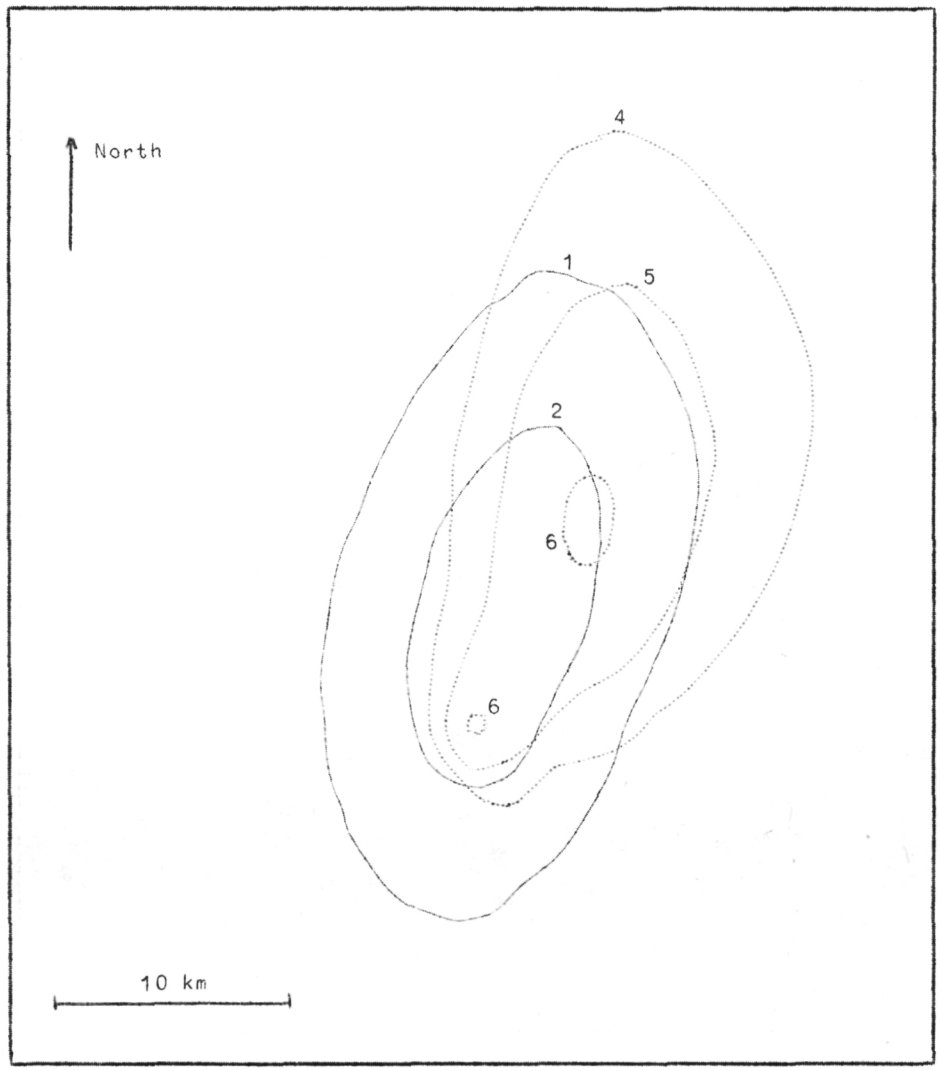

fig. 13.
Isoconcentrations $\frac{3}{4}$ tidal period of the release.

i) a rapid decrease of the total quantity of suspensions despite a periodic recirculation of depositing sediments associated with the stronger tidal currents (the partial recirculation is reflected by the regular bumps in the curve of overall decay);

ii) a strongly anisotropic dispersion characteristic of the shear effect and manifested by the elongation of the isoconcentration curves along the great tidal axis;

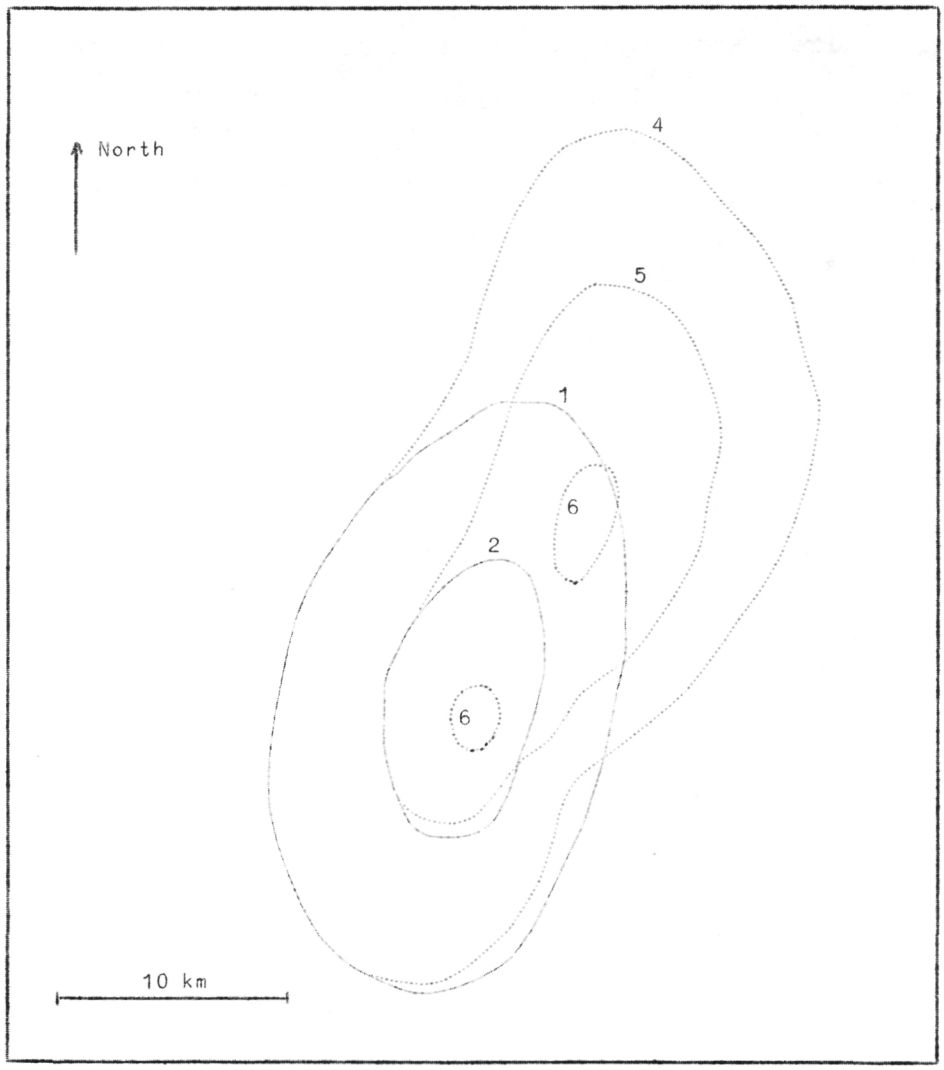

fig. 14.
Isoconcentrations 1 tidal period after the release.

iii) the tendency of the curves of equal concentrations of suspensions to take, *after one tidal period*, quasi-elliptical forms roughly centered at the dumping point. This final shape can be predicted by a simplified model where the evolution equations are, to begin with, integrated over a tidal period [Nihoul (1975a)];

iv) the division of curve 6 (500 mg/m^2) in two and the appearance of a second zone of high sediments-concentration to the north-east of the dumping area. This factor, combined with a general north-east bound

residual current in the area, can be associated with the observed progressive displacement of the deposited dumped material towards the north-east.

VI.- BOTTOM EROSION

Based on :

- LAMBERMONT J. and LEBON G. (1974), Erosion of cohesive soils, Programme national sur l'environnement physique et biologique, C.I.P.S., N 40.

1.- Introduction

Sedimentation means the transport of matter through a solution due to an external force field. Thereby sediment layers are built up at the bottom region of rivers, estuaries and oceans. Depending on the friction velocity or shear stress acting at the layer, deposition or erosion occurs.

Knowledge of the erosion flux under varying flow conditions is important in such diverse areas as estuary maintenance, channel design and pollution dispersal in rivers and oceans.

The results provided by mathematical marine models are only truthworthy when correct boundary inputs are known [Nihoul (1975a)], *i.e.* when the erosion flux is related to the fluid flow.

Many investigations have been carried out on the transport of sand beds (which is not a pollutant) but relatively little has been done on muds. Particularly in pollution studies it is mandatory to have information on the settling and scouring rates of fine grained particles [McCave (1972)].

In this section we concentrate on the physical behaviour of the visco-plastic sediment layer and derive the expression for the erosion flux by considering the action of the turbulent flow.

In § 2, the mass conservation law for a sediment bed is formulated. In § 3, the boundary condition at the bed-fluid interface is discussed; use is made of the experimental data of Migniot (1968). The density distribution is discussed in § 4 and the interface mass flux continuity in § 5. In § 6, the analytic solution for the stationary erosion flux is obtained which for a fine grained sediment can be simplified (§ 7). In § 8, the theory is shown to describe very accurately the experimental studies performed by Partheniades (1965).

2.- Mass conservation law for the sediment bed

Consider a dynamically smooth and isotropic viscoplastic sediment layer (sea bed) in a gravitational field acted on by a two-dimensional turbulent fluid flow.

For simplicity we consider a two component non charged chemically non reacting system, for example water and a single component fine grained sediment as clay.

The solid particle or sediment mass flux $\mathbf{J}^s$ with respect to the barycentric velocity $\mathbf{v}$ of the bed is defined by

$$\mathbf{J}^s = \rho^s(\mathbf{v}^s - \mathbf{v}) \tag{10}$$

where ρ^s and $\mathbf{v}^s$ are the solid particle density and velocity.

The mass conservation equation for the sediment component reads

$$\frac{\partial \rho^s}{\partial t} = - \nabla . (\rho^s \mathbf{v}^s) \quad . \tag{11}$$

Substituting (10) into (11) gives :

$$\frac{\partial \rho^s}{\partial t} = - \nabla . \mathbf{J}^s - \nabla . (\rho^s \mathbf{v}) \quad . \tag{12}$$

We shall neglect temperature gradients in the sediment layer.

Further we consider throughout the layer constant diffusion D^s and sedimentation S^s coefficients. The sediment mass flux with respect to the barycentric velocity is in this case given by :

$$\mathbf{J}^s = - D^s \nabla \rho^s + S^s \rho^s \mathbf{g} \quad . \tag{13}$$

Substituting (13) in (12) results in

$$\frac{\partial \rho^s}{\partial t} = D^s \nabla^2 \rho^s - S^s \mathbf{g} . \nabla \rho^s - \nabla . (\rho^s \mathbf{v}) \quad . \tag{14}$$

These equations are formally the same as for a fluid. However, the sediment layer differs from a fluid — the latter cannot by definition support a shear stress at equilibrium — in that it shows viscoplastic behaviour, *i.e.* possesses a yield stress. That is to say, under an

applied shear stress less or equal to the yield shear stress, it behaves like an elastic solid while above this stress it shows a rate of deformation which is a function of the difference between the applied and yield stresses. The yield stress is a function of the solid component density which varies through the depth of the sediment layer.

Introducing a coordinate system wherein the z axis points downwards normal to the interface between the fluid and flat sediment layer, we consider a sediment layer in which the solid particle density depends only on z and t. The fluid flow above it is turbulent and two-dimensional. Apart from a hydrostatic pressure the fluid exerts then only a shear stress to the top of the sea or river bed.

Consequently plastic shear deformation in the sediment layer is, if it occurs, parallel to the x-y plane. A reasonable approximation inside the layer is then to assume that the barycentric velocity component in the z direction is negligibly small while its other two components are functions of z and t only. Under these restrictions (14) reduces to :

$$\frac{\partial \rho}{\partial t} = D \frac{\partial^2 \rho}{\partial z^2} - S\, g_z \frac{\partial \rho}{\partial z} \tag{15}$$

wherein we have omitted the superscript s.

The z component of (13) is

$$J_z = - D \frac{\partial \rho}{\partial z} + S\, \rho\, g_z \,. \tag{16}$$

3.- The boundary condition at the bed-fluid interface

According to Migniot (1968) the shear stress whereby erosion finds place is uniquely related to the yield stress. Tentatively we shall assume this to be true. Thus for a given sediment layer, with solid particle density ρ_c at the top, erosion finds place when the shear stress exerted on it by the fluid reaches a certain critical value.

To make this statement explicit let us reproduce the experimental results found by Migniot.

The yield shear stress τ_y is, for a great variety of muds, experimentally found to be related to the solid density ρ by

$$\tau_y = n\,\rho^m \tag{17}$$

where n and m are constants depending on the soil. When τ_y is expressed in N/m^2 and ρ in g/ℓ Migniot found m to be close to 5 for all cohesive soils examined while n varies from 10^{-12} to 10^{-15}, depending on the particular sediment.

The yield stress at the top of the sediment layer, where $\rho = \rho_c$, is thus

$$\tau_y = n\,\rho_c^m \quad . \tag{18}$$

Further it is found experimentally that the critical friction velocity U_* acting at the sediment layer, whereby erosion finds place is related to the yield stress by :

$$\begin{cases} U_{*c}(\text{cm/s}) = \tau_y^{1/4}(\text{dynes/cm}^2) & \text{for } \tau_y \leq 15 \text{ dynes/cm}^2 \\ U_{*c}(\text{cm/s}) = 0.5\,\tau_y^{1/2}(\text{dynes/cm}^2) & \text{for } \tau_y \geq 15 \text{ dynes/cm}^2 \end{cases} \tag{19}$$

In M.K.S. units, one has :

$$\begin{cases} U_{*c}(\text{m/s}) = 0.01778\,\tau_y^{1/4}(\text{N/m}^2) & \text{for } \tau_y \leq 1{,}5 \text{ N/m}^2 \\ U_{*c}(\text{m/s}) = 0.016\,\tau_y^{1/2}(\text{N/m}^2) & \text{for } \tau_y \geq 1{,}5 \text{ N/m}^2 \end{cases} \tag{20}$$

Figure 15, taken from Migniot (1968), shows how the relations (20) compare with the experimental points obtained for a number of sediments.

There is a remark to be made here. We infer from the experiments performed by Migniot that τ_y appearing in (19) is the average shear yield stress of the bed in the upper region (say 1 to 10 cm) of the layer. The contact with the fluid will lower the solid particle density and thus by (13) also the yield stress at the top of the sediment layer by a factor G, which we expect to have a value between 1 and 5 .

Taking this into account we obtain from (17) and (20) :

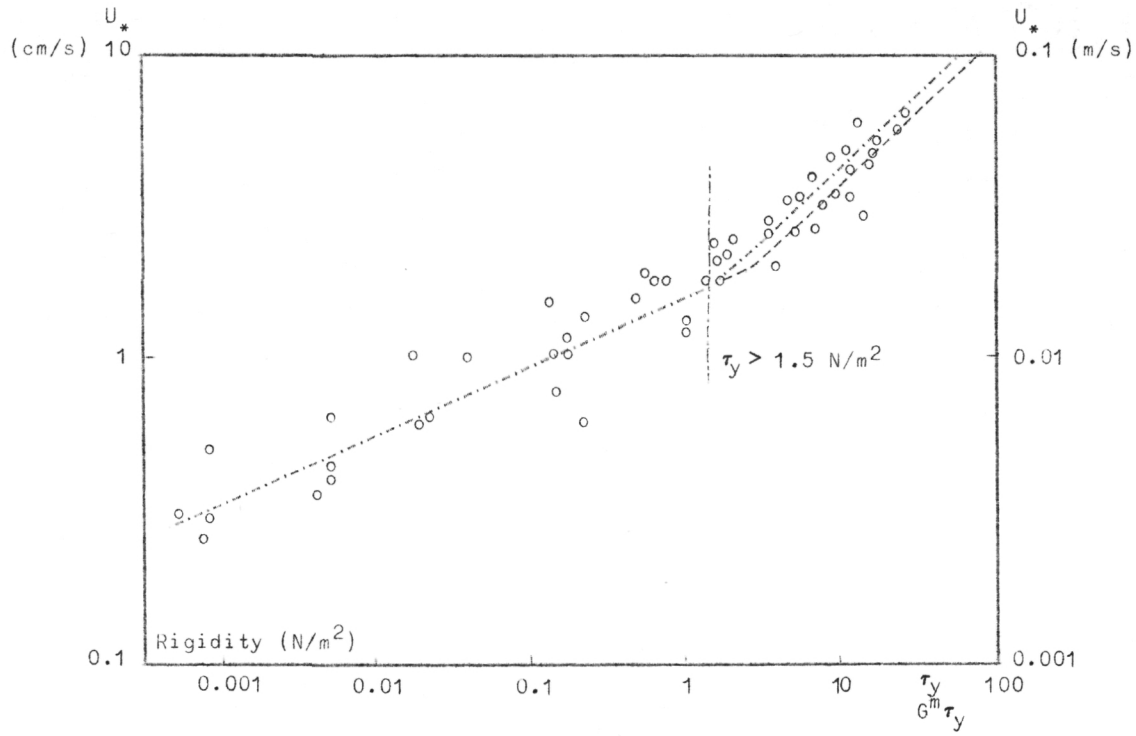

fig. 15.

Critical friction velocity U_* versus yield stress τ_y in upper sediment bed region (after Migniot). The yield stress at the top of the sediment bed $G^m\tau_y$ is also shown.

(21)
$$\begin{cases} U_{*_c}(m/s) = 0.0178\ G^{m/4}\tau_y^{1/4}\ (N/m^2) & \text{for } \tau_y \leq \dfrac{1.5}{G^m}\ N/m^2 \\ U_{*_c}(m/s) = 0.016\ G^{m/2}\ \tau_y^{1/2}\ (N/m^2) & \text{for } \tau_y \geq \dfrac{1.5}{G^m}\ N/m^2 \end{cases}$$

where τ_y is now the yield shear stress at the top of the bed. It is clear from (20) and (21) that Migniot's figure (fig. 15) describes correctly the relation (21) when the absciss in that figure is replaced by $G^m\tau_y$.

The relations (21) may be written as :

(22) $$U_{*_c} = p_i\ \tau_y^{q_i} \qquad (i = 1,2)$$

where $i = 1$ in region 1, defined for $\tau_y \leq \dfrac{1.5}{G^m}\ N/m^2$, and $i = 2$ in region 2, defined for $\tau_y \geq \dfrac{1.5}{G^m}\ N/m^2$.

The critical friction velocity is related to the shear stress exerted by the fluid whereby erosion finds place by :

(23) $$U_{*c} = \sqrt{\frac{\tau}{\rho_v}}$$

wherein ρ_v is the fluid density in the viscous sublayer.

Combining (18), (22) and (23) one finds the relation between the shear stress whereby erosion finds place and the instantaneous value of the solid particle density at the top of the bed, ρ_c, *i.e.*

(24) $$\tau = E_i \, \rho_c^{B_i} \qquad (i = 1,2)$$

where $$E_i = \rho_v \, p_i^2 \, n^{2q_i} \qquad B_i = 2\,mq_i \; .$$

The relations (20), (21), (22) and hence (24) have been determined under quasi-stationary experiments and may consequently not apply to rapidly varying bed shear stress.

Partheniades (1965) has criticized the existence of a relation between a critical friction velocity or shear stress whereby erosion occurs and the yield stress at the top of the bed. From experiments he found that dissolving iron oxides into a sediment layer does not noticeably change the macroscopic shear stress but changes the bed stress whereby erosion occurs. In what follows it will become clear that it is only essential that a relation of the type (24) exists while a relation as (22) need not be true. That is to say, we demand that the instantaneous physico-chemical composition at the top of the sediment bed determines uniquely the bed shear stress whereby scouring (erosion) occurs. Let us observe that the bed shear stress necessary for erosion depends also on the particle density in the viscous sublayer via ρ_v appearing in (24). However the variation of ρ_v with particle density is rather small. This agrees with the observation of Partheniades that the erosion rate is practically independent of the average particle density in the fluid for the range up to 12 g/ℓ attained in his experiments.

Suppose that after some time during which a sediment layer has built up by deposition, the shear stress is rather suddenly raised, say, due to the occurence of a storm. It is clear from (24) that in a short time the sea bed will be eroded to the depth where the solid concentration corresponds to the critical density. During such change one expects

a high scouring rate or even the formation of mud pebbles entering the fluid. This has indeed been observed [Migniot (1968), Partheniades (1972)].

We focus our attention on the calculation of the erosion flux which occurs from there on, when the applied shear stress is either constant (steady state) or changes quasi-stationary. Thereto (15) has to be solved under the appropriate initial and boundary conditions.

4.- The density distribution in a cohesive sediment bed

The initial condition of the sediment layer depends strictly speaking on the whole previous deposition and erosion history.

Nevertheless one can form a reasonable good idea of the solid particle density through the sediment layer from experiments in the ultracentrifuge where processes are speeded up enormously. Figure 16, taken from Fujita (1962), shows how the solid particle density distribution ρ changes in a centrifuge with inner radius r_1 and outer radius

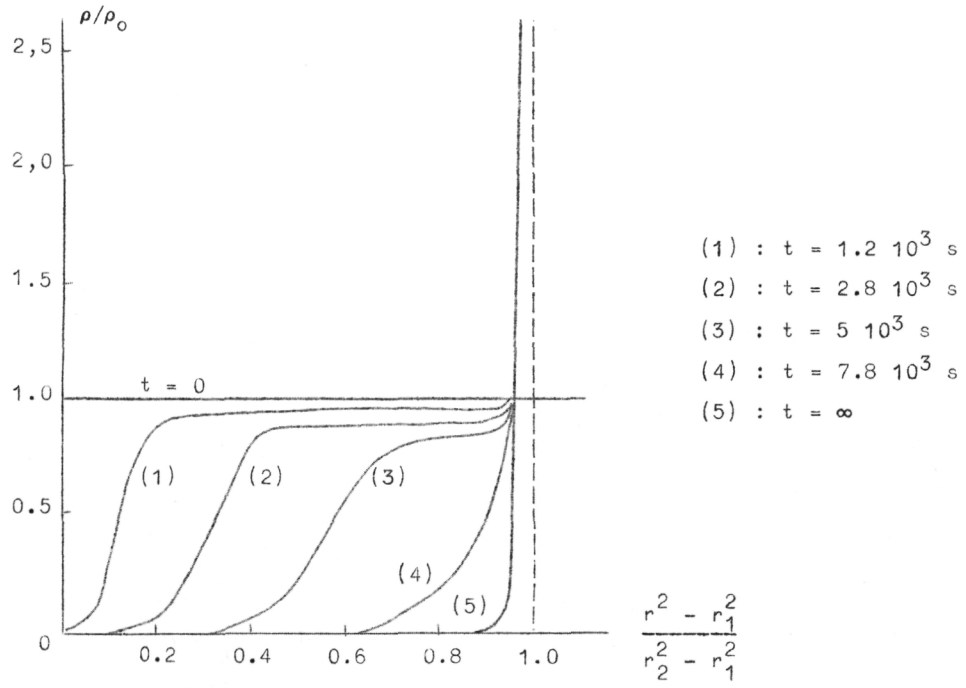

fig. 16.
Variation of density distribution in the ultra centrifuge (after Fujita).

r_2 . The (constant) angular velocity is ω and initially the two components fluid is homogeneous with a sediment density ρ_0 .

The important thing to observe is that for a rather long time one observes a sediment density distribution having a "plateau" region and that the change in plateau density value varies only slowly with time. Migniot (1968) who performed experiments on the settling of solid particles in a gravitational field found also the distribution with a near "plateau" region.

Guided by these results we assume a solid particle density distribution as shown in figure 17 and assume that the density ρ_p at the

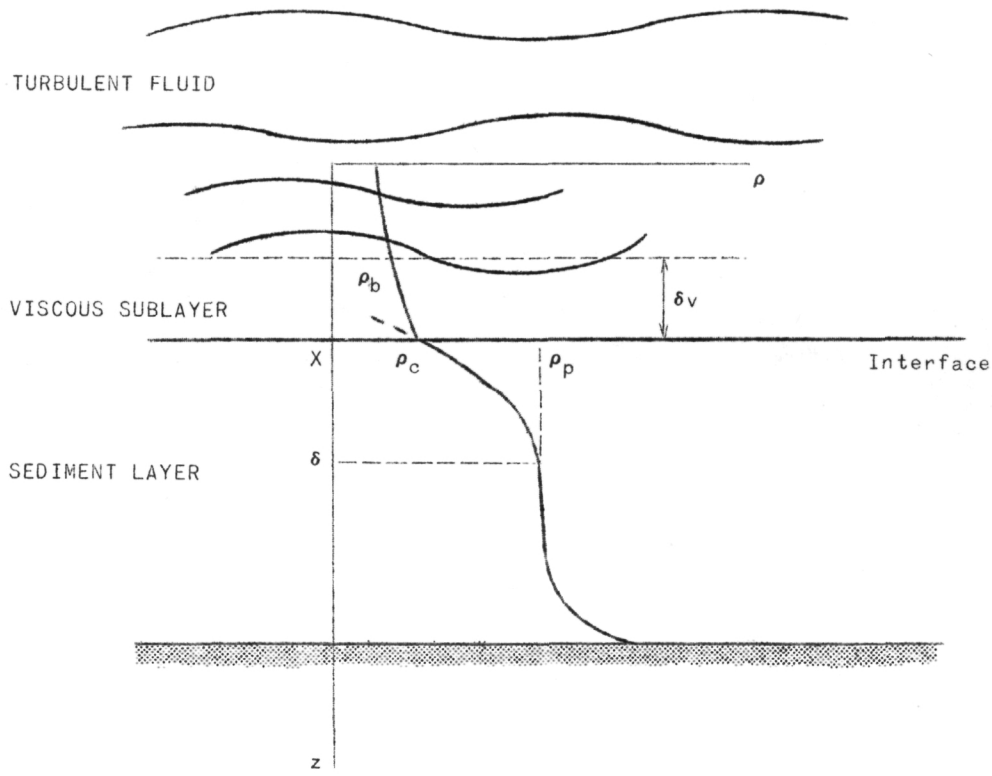

fig. 17.
Density distribution in the sediment bed.

"plateau", at $z = \delta$, remains constant during erosion. The density at the fluid-bed interface at $z = X$, is denoted by ρ_c . As long as erosion occurs its value is determined by (24), *i.e.* by the shear stress acting at the interface.

The vertical profile shown in figure 17 corresponds with the experimentally observed dissolved silica concentration in the North Sea [Wollast and Van Der Borght (1974)].

For $X \leq z \leq \delta$ a parabolic sediment density distribution of the following form may be assumed :

$$\rho = \rho_p + (\rho_c - \rho_p)\left(1 - \frac{z - X}{\delta - X}\right)^2 \qquad X \leq z \leq \delta \tag{25}$$

which satisfies

$$\begin{aligned} &\rho = \rho_c && && \text{at} && z = X \\ &\rho = \rho_p && \text{and} && \frac{\partial \rho}{\partial z}(\delta, t) = 0 && \text{at} && z = \delta \end{aligned} \tag{26}$$

5.- The interface mass flux continuity

In (25), X and δ are, of course, unknown functions of the time. To determine them with (15) we need one additional boundary condition. Thereto we set up the mass balance equation at the interface. Denote by J_+^* the sediment flux *with respect to the moving interface* in the sediment layer arbitrarily close to $X(t)$ and by J_-^* its value in the fluid arbitrarily close to $X(t)$.

By definition one has :

$$J_-^* = \rho_c^s \left(\mathbf{v}_-^s - \frac{dX}{dt}\right) \quad ; \quad J_+^* = \rho_c^s \left(\mathbf{v}_+^s - \frac{dX}{dt}\right) \tag{27}$$

where $\mathbf{v}_+^s$ and $\mathbf{v}_-^s$ are the velocities of the sediment contaminant in the sediment layer and fluid respectively and $\frac{dX}{dt}$ is the velocity of the interface.

The z components of these fluxes are :

$$J_{-z}^* = \rho_c^s \left(v_-^s - \frac{dX}{dt}\right) \quad , \quad J_{+z}^* = \rho_c^s \left(v_+^s - \frac{dX}{dt}\right) . \tag{28}$$

The sediment flux, in the sediment layer arbitrarily close to the interface, with respect to the barycentric or center of mass velocity $\mathbf{v}_+$ is by definition :

(29) $$\mathbf{J} = \rho_c^s \, (\mathbf{v}^s - \mathbf{v}_+)$$

Its z component is

(30) $$J_z = \rho_c^s \, (v^s - v_+) \, .$$

Combining (28) and (30) one obtains for the erosion flux counted positi e downwards

(31) $$J_z = J^*_{+z} + \rho_c^s \, (\frac{dX}{dt} - v_+) \simeq J^*_{+z} + \rho_c^s \, \frac{dX}{dt} \, .$$

The approximation expresses that the barycentric velocity in the sediment layer is negligible compared to $\frac{dX}{dt}$.

As there are no sources or sinks at the bed-fluid interface the normal sediment flux across it measured with respect to the interface velocity must be continuous, so that

$$J^*_{-z} = J^*_{+z} \equiv J_{z,v} \, .$$

Hence (31) can be written, omitting the superscript s ,

$$J_z = J_{z,v} + \rho_c \, \frac{dX}{dt} = \sigma \, \rho_c - D \, \frac{\partial \rho}{\partial t} \, (X,t) \, .$$

Here, (16) has been used and we have put $\sigma = s \, g_z$ where σ is the settle particle velocity in the sediment layer.

To determine the flux $J_{z,v}$ which crosses from the fluid to the sediment layer we calculate the diffusion and the sedimentation fluxes through the viscous sublayer.

The flow in the viscous sublayer is laminar-like in that the mean velocity profile is identical to the linear velocity profile of a plane parallel laminar flow with zero pressure gradient [Monin (1965)]. Nevertheless the flow is three-dimensional and unsteady [Kline *et al.* (1967)] . Streaks were observed by them to waver and oscillate and to pass sometimes rapidly to the outer edge of the boundary layer. The continuous formation and break up of low speed streaks fluctuations, which increase the diffusion coefficient to a higher value than the molecular one, presumably become more frequent and larger with increasing Reynolds number.

We denote the solid particle density (mass of sediment per unit fluid volume) at the top of the viscous sublayer, where it meets the logarithmic boundary layer, by ρ_b (see fig. 17).

The diffusion flux through the viscous sublayer with respect to the interface velocity, counted positive downwards, may be expressed by

$$\hat{J}_{z,diff} = - L (\rho_c - \rho_b) \tag{33}$$

wherein the transport coefficient L is defined by

$$L = \frac{D_v}{\delta_v} > 0 \tag{34}$$

where D_v is the diffusion coefficient and δ_v the thickness of the sublayer.

In (33) we have assumed that the solid particle density varies linearly through the viscous sublayer.

In addition to this diffusion flux there is a sediment flux through the viscous sublayer. Its average, counted positive downwards is

$$\hat{J}_{z,sed} = \frac{1}{\delta_v} \int_0^{\delta_v} J_{z,sed}\, dz = \frac{1}{\delta_v} \int_0^{\delta_v} \sigma_v\, \rho\, dz = \frac{1}{2}\, \sigma_v\, (\rho_b + \rho_c) \tag{35}$$

The total flux through the sublayer, counted positive downwards, is found by adding (33) and (35) :

$$J_{z,v} = L (\rho_b - \rho_c) + \frac{1}{2}\, \sigma_v\, (\rho_b + \rho_c) \,. \tag{36}$$

The viscous sublayer thickness appearing in (34) is related to the critical friction velocity U_{*c}, the fluid kinematic viscosity and the fluid density ρ_v [Monin (1965)] :

$$\delta_v = \alpha_v \frac{\nu}{U_{*c}} = \alpha_v\, \nu \sqrt{\frac{\rho_v}{\tau}} \tag{37}$$

where τ is the critical shear stress acting at the interface between fluid and sediment layer and α_v is a universal constant of order unity.

Hence

$$L = \frac{D_v\, U_{*c}}{\alpha_v\, \nu} = \frac{D_v}{\alpha_v\, \nu}\, \rho_v^{-\frac{1}{2}}\, \tau^{\frac{1}{2}} \,. \tag{38}$$

The relation (32) with $J_{z,v}$ given by (36) and the L appearing herein by (38) determine the additional boundary condition to (26). With them we shall proceed to solve the differential equation (15); its solution is approximated by assuming the parabolic distribution given by (24) and yields the erosion flux.

6.- The solution for the erosion flux

Integration of (15) between $z = X$ and $z = \delta$ results in

$$\int_{X(t)}^{\delta(t)} \frac{\partial \rho}{\partial t}\, dz = -\sigma \int_{X(t)}^{\delta(t)} \frac{\partial \rho}{\partial z}\, dz + D \int_{X(t)}^{\delta(t)} \frac{\partial^2 \rho}{\partial z^2}\, dz$$

$$\int_{X(t)}^{\delta(t)} \frac{\partial \rho}{\partial t}\, dz = -\sigma\,(\rho_p - \rho_c) + \frac{2\,D}{\delta - X}\,(\rho_c - \rho_p) \tag{39}$$

where we have made use of $\frac{\partial \rho}{\partial z}(\delta,t) = 0$ and

$$\frac{\partial \rho}{\partial z}(X,t) = -\frac{2}{\delta - X}\,(\rho_c - \rho_p) \tag{40}$$

which follows from (25).

Now by Leibnitz's rule we have

$$\frac{d}{dt} \int_{X(t)}^{\delta(t)} \rho(z,t)\, dz = \int_X^{\delta} \frac{\partial \rho}{\partial t}\, dz + \rho(\delta,t)\, \frac{d\delta}{dt} - \rho(X,t)\, \frac{dX}{dt}\,. \tag{41}$$

Combining (39) and (41) and using (26) gives

$$\frac{d}{dt} \int_X^{\delta} \rho\, dz = \rho_p\, \frac{d\delta}{dt} - \rho_c\, \frac{dX}{dt} + \sigma\,(\rho_c - \rho_p) + \frac{2\,D}{\delta - X}\,(\rho_c - \rho_p)\,. \tag{42}$$

We proceed to evaluate the left hand side of this equation by means of (25). We find

$$\int_X^{\delta} \rho\, dz = \frac{\delta - X}{3}\,(2\,\rho_p + \rho_c)\,. \tag{43}$$

We have pointed out that it is a good approximation to assume that ρ_p is constant, see figure 16. For a *steady* erosion flux which requires a constant applied shear stress at the top of the viscoplastic sediment layer one finds from (24) that ρ_c is constant. Hence

$$(44) \qquad \frac{d}{dt}\int_{\chi}^{\delta} \rho \, dz = \left(\frac{d\delta}{dt} - \frac{dX}{dt}\right)\left(\frac{2\,\rho_p + \rho_c}{3}\right) .$$

Thus for this case (42) reduces to :

$$(45) \qquad \frac{2\,\rho_p + \rho_c}{3}\left(\frac{d\delta}{dt} - \frac{dX}{dt}\right) = \rho_p \frac{d\delta}{dt} - \rho_c \frac{dX}{dt} + \sigma\,(\rho_c - \rho_p) + \frac{2\,D}{\delta - X}(\rho_c - \rho_p) .$$

In addition to this relation we obtain a second one when (40) is substituted in (32) :

$$(46) \qquad J_z = J_{z,v} + \rho_c \frac{dX}{dt}$$

$$(47) \qquad = \sigma\,\rho_c + 2\,D\,\frac{\rho_c - \rho_p}{\delta - X} .$$

In the stationary state J_z and $J_{z,v}$ are constant. Hence it follows from (46) that $\frac{dX}{dt}$ must be constant. It follows now from (47) that $\delta - X$ must also be constant.

Thus

$$(48) \qquad \frac{d\delta}{dt} = \frac{dX}{dt} .$$

Whence for the stationary state we obtain from (45)

$$(49) \qquad (\rho_c - \rho_p)\frac{dX}{dt} = \sigma\,(\rho_c - \rho_p) + \frac{2\,D}{\delta - X}(\rho_c - \rho_p) .$$

Eliminating $\frac{2\,D}{\delta - X}(\rho_c - \rho_p)$ between (47) and (49) gives

$$(50) \qquad \frac{dX}{dt} = \sigma - \frac{J_{z,v}}{\rho_p} .$$

Substituting this result in (46) gives for the stationary erosion flux :

$$(51) \qquad J_z = \rho_c\,\sigma + \left(1 - \frac{\rho_c}{\rho_p}\right) J_{z,v} .$$

The erosion flux, J , for the stationary state counted as *positive upwards, i.e.* $J = -J_z$, is finally found when (36) is substituted into (51). One has :

$$(52) \qquad J = -\rho_c\,\sigma + \left(\frac{\rho_c}{\rho_p} - 1\right)\left[L\,(\rho_b - \rho_c) + \frac{1}{2}\sigma_v\,(\rho_b + \rho_c)\right]$$

wherein

(53) $$\rho_c = \left(\frac{\tau}{E_i}\right)^{1/B_i}$$

as follows from (24). L which is also a function of τ is given by (38).

The equation (52) has been derived under the assumption that erosion occurs. The auxiliary condition herefore is as follows : when the instantaneous solid particle density at the top of the bed is ρ_c then erosion finds place if and only if the bed shear stress is larger or equal to the critical value τ determined by (53).

This loading condition can also be referred to the initial bed state. Consider a fluid flow such that no erosion finds place. (Either sediment deposition finds place or no deposition and no erosion.) Denote the sediment density at the top of the sediment bed in this state by ρ_1 . The minimum shear stress necessary for the onset of erosion follows from (24) as

(54) $$\tau_1 = E_1 \rho_1^{B_1} \quad .$$

For a shear stress which is smaller but arbitrarily close to τ_1 no erosion occurs. Thus (52) gives the steady state erosion flux for $\tau \geq \tau_1$.

It is clear that the analysis implies that when the bed shear stress is decreased, erosion will cease at once.

Scouring will reoccur under this lower shear stress when the density at the top of the bed diminishes until a value is reached which corresponds with the new ρ_c determined by (53). The lowering of the density during the period when no erosion occurs is due to the diffusion of water into the sediment bed. From the other side deposition will counteract by increasing the bed density. However the experiments of Partheniades show that the latter effect is negligible, because lowering of the shear stress results, in a very short time during which settling is negligible, in a lower scouring rate determined by (52). Settling will only occur when the bed stress is lowered to a minimum value which is close to the value τ_1 at which scouring is first observed for a fresh sediment bed.

7.- An approximate expression of the erosion flux

A simplification of the relation (52) is possible when the defloccu-lated solid particle diameter is very small. During stationary erosion the solid particles break continuously from the bed. Thus unlike deposition during which the particles are flocculated, the diameter of the particles passing during erosion through the viscous sublayer to the bulk fluid is likely to be very small. Therefore the settle velocity in the viscous sublayer approaches a negligible value. This is in accordance with the observations that single clay particles can be carried in suspension by Brownian motion.

The settling velocity σ_v during erosion we expect therefore to be much smaller than $L = \frac{D_v}{\delta_v}$.

The latter is of the order 10^{-9} m/s (the molecular diffusion $D_v \simeq 10^{-11}$ m^2/s while $\delta_v \simeq 0.01$ m).

Hence, for fine grained cohesive soils

$$L \gg \sigma_v \quad , \quad L \gg \sigma \; . \tag{56}$$

The solid particle density at the top of the sediment layer ρ_c is during erosion related to the bed shear stress τ by the relation (53). The condition

$$\frac{\rho_c}{\rho_p} \ll 1 \tag{57}$$

is therefore expected to be satisfied for sufficiently small bed shear stresses. Under the conditions (56) and (57), (52) reduces to :

$$J_i = \frac{L}{E_i^{1/B_i}} \left(\tau^{1/B_i} - \rho_b \, E_i^{1/B_i}\right) \quad \text{for} \quad \tau \geq \tau_1 \quad (i = 1,2) \; . \tag{58}$$

As $J_1 = 0$ for $\tau = \tau_1$ we have

$$\tau_1^{1/B_i} = \rho_b \, E_1^{1/B_i} \; .$$

Hence we may write

$$J_i = \frac{L}{E_i^{1/B_i}} \left(\tau^{1/B_i} - \tau_i^{1/B_i}\right) \quad \text{for} \quad \tau \geq \tau_i \quad (i = 1,2) \; . \tag{59}$$

Thus

$$J_1 = \frac{L}{E^{1/B_1}} \left(\tau^{1/B_1} - \tau_1^{1/B_1}\right) \tag{60}$$

for region 1. One may introduce a bed shear stress τ_2 whereby the flux in region 2 would be zero if only region 2 would be present. That is to say, when only the straight line describing the second region in figure 15 is considered with the understanding that this line is prolonged to cut the absciss. Hence

$$J_2 = \frac{L}{E^{1/B_2}} \left(\tau^{1/B_2} - \tau_2^{1/B_2}\right) \tag{61}$$

in region 2 .

Substituting (34), (37) into (59) yields for the erosion flux

$$J_i = A_i \left(\tau^{1/B_i} - \tau_i^{1/B_i}\right)\tau^{\frac{1}{2}} \quad \text{for} \quad \tau \geq \tau_i \quad (i = 1,2) \tag{62}$$

where

$$A_i = \frac{D_v}{\alpha_v \nu \rho_v^{\frac{1}{2}} E_i^{1/B_i}} \,. \tag{63}$$

The constants appearing herein differ in the first region $(i = 1)$ and second region $(i = 2)$ according to (21) - (24).

It is interesting to observe that for $B_i = 1$, (62) reduces to the bed-load relation derived by Bagnold (1956), see also Monin (1965), for a sand bed. The quantity A_1 is there not determined from the theory but taken from an experimental graph where it is plotted against sand particle diameter.

Of course, the equations we have derived should apply equally to the flow of air over a dust layer, at least when the latter has similar properties as the sediment layer we considered above.

8.- Comparison with experiment

Partheniades (1965), (1972), conducted laboratory erosion experiments in an open rectangular channel. We quote him for the following facts.

"The experiments were conducted in an open flume with recirculating water at ocean salinity. The bed material, sampled from the San Francisco Bay and known as Bay mud, contained approximately equal amounts of silt and clay and some traces of fine sand and organic matter. It is a highly plastic soil with a liquid limit of 99 % and a plasticity index (PI) of 55 % . The clay proportion consists predominantly of montmorillonite and illite. Figure 18 shows the erosion rate as function of the average bottom shear stress. Series I correspond with a bed remolded at its field moisture of 110 % with a shear strength of about 20 p.s.f. ($\simeq$ 1000 N/m^2) at ultimate failure and 11 p.s.f. at yield point. The minimum bed shear strength at which erosion was first observed was about 0.002 p.s.f. ($\simeq$ 0.1 N/m^2) . The bed in series II was formed by releveling that of series I. However, due to some unavoidable water entrainment, it displayed a higher water content and lower shear strength. The observed increase of the resistance to erosion was attributed to cementation due to iron oxides dissolved in the water. The fact that the increased interparticle bonds were not reflected in the macroscopic shear strength of the bed indicates that the soil cohesion, as determined by conventional shear strength tests, is not a representative or a unique measure of the soil resistance to erosion".

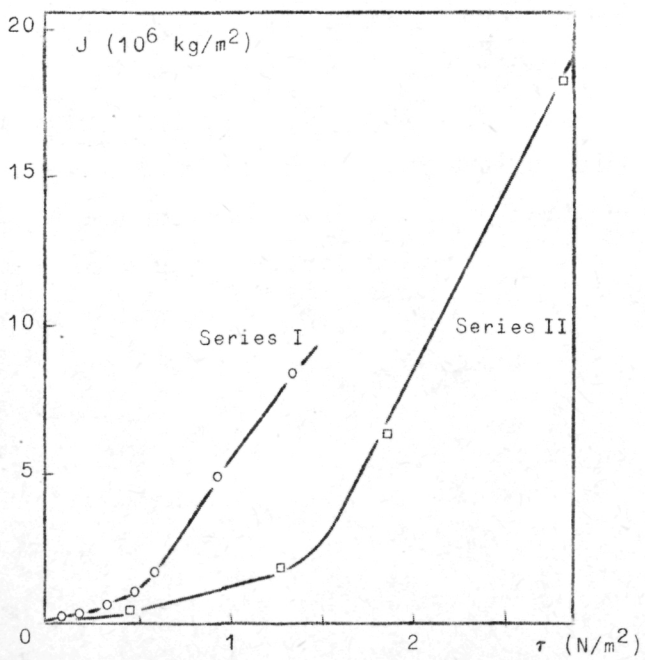

fig. 18.
Variation of erosion rates J with bottom shear stress τ (after Partheniades).

We have commented that a unique relation between the critical shear stress and yield stress is not essential for the theory. The essential thing is that the instantaneous physico-chemical composition at the top of the sediment layer (at the sediment-fluid interface) determines uniquely the shear stress whereby erosion finds place.

To apply the relation (62) to the experiments performed by Partheniades we shall assume that the Bay mud has properties which correspond closely to the data given by Migniot for the Provins clay. For that mud $m = 5$ and $n \simeq 10^{-13}$.

The shear stress whereby erosion occurs is related to the yield stress at the top of the sediment layer by

$$\tau = \rho_v \, p_1^2 \, \tau_y^{2q_i} \tag{64}$$

as follows from (22) and (23).

Series I

There is a clear change in the nature of series I, figure 18, for a bed shear stress of about $\tau_c = 0.011$ lb/ft^2 $= 0.53$ N/m^2 . Using this value in (64) and $\rho_v \simeq 1000$ kg/m^3 and the values $p_1 = 0.0178 \, G^{5/4}$, $q_1 = 0.25$ found by Migniot for the first region [for completeness we shall carry the correction factor introduced in (21) along], we find for the corresponding yield stress $\tau_y = \frac{2.7}{G^5}$ N/m^2 .

By inspection of figure 15 it is seen that this value corresponds very well to the intersecting point of the two straight lines if the line for the higher yield stress range (region 2) is drawn through the experimental points of the Provins clay. The equation for this second line is ($m = 5$) :

$$U^* = p_2 \, \tau_y^{q_2} = 0.0139 \, G^{5/2} \, \tau_y^{0.5} \, .$$

Accordingly, we shall use the values :

$$\begin{cases} p_1 = 0.0178 \, G^{5/4} \quad , \quad q_1 = 0.25 \\ p_2 = 0.0139 \, G^{5/2} \quad , \quad q_2 = 0.5 \end{cases} \tag{65}$$

With (65) it follows from (64) that the two regions are separated at the bed shear stress $\tau = 0.53\ N/m^2$.

From (65) and (24) it follows that

(66) $$B_1 = 2.5 \quad , \quad B_2 = 5 \ .$$

The erosion relation (62) becomes now

(67) $$J_1 = A_1 (\tau^{0.4} - \tau_1^{0.4})\ \tau^{0.5} \quad \text{for} \quad 0.12\ N/m^2 \le \tau \le 0.53\ N/m^2$$

(68) $$J_2 = A_2 (\tau^{0.2} - \tau_2^{0.2})\ \tau^{0.5} \quad \text{for} \quad \tau \ge 0.53\ N/m^2$$

The initial critical bed shear stress reported by Partheniades whereby erosion occurs is $\tau_1 = 0.0025\ lb/ft^2 = 0.12\ N/m^2$.

Using the experimental values

$$J_1 = 0.435\ g/ft^2.h = 1.3 \times 10^{-6}\ kg/m^2.s \quad \text{for} \quad \tau = 0.53\ N/m^2$$

and

$$J_2 = 2.46\ g/ft^2.h = 7.37 \times 10^{-6}\ kg/m^2.s \quad \text{when} \quad \tau = 0.025\ lb/ft^2 = 1.197\ N/m^2$$

obtained from figure 18; we determine the constants in (67) and (68) as

(69)
$$\tau_1 = 0.12\ N/m^2 \quad , \quad \tau_1^{0.4} = 0.43 \quad , \quad A_1 = 4.96 \times 10^{-6}$$
$$\tau_2 = 0.39\ N/m^2 \quad , \quad \tau_2^{0.2} = 0.83 \quad , \quad A_2 = 33 \times 10^{-6}$$

The calculated curve in figure 18 shows that with these values, (67) and (68) give a remarkable good description of the erosion flux observed in series I. In particular one notes that the change in slope is predicted by the theory.

To confirm the theory we must however check if, with the A's given by (69), the diffusion coefficient in the viscous sublayer calculated with (63) corresponds in order of magnitude with the molecular diffusion coefficient $10^{-10} - 10^{-11}\ m^2/s$.

For the two regions we obtain from (24), taking $\rho_v = 1000\ kg/m^3$:

(70) $$E_1 = 10^{-7}\ G^{5/2} \quad , \quad E_2 = 1.93 \times 10^{-14}\ G^5 \ .$$

Using $\alpha_v \simeq 10$, $\nu = 10^{-5}\ m^2/s$ we find from (63) :

$$D_v = 2.4 \times 10^{-11}\ G\ m^2/s \quad \text{in region 1 ,}$$

$$D_v = 1.9 \times 10^{-11}\ G^2\ m^2/s \quad \text{in region 2 .}$$

These diffusion coefficients are of the same order. For a correction factor $G = 5$, the average diffusion coefficient in region 2 is about four times that in region 1. As the turbulent fluctuations in the viscous sublayer become presumably more frequent with increasing shear stress it must be expected that the diffusion coefficient becomes larger.

Series II

Partheniades reports that the increased resistance against erosion in series II is believed to be caused by dissolved iron oxides.

Figure 18 shows that a strong increase in the erosion rate occurs for this II bed by a shear stress of about $\tau = 0.031\ lb/ft^2 = 1.48\ N/m^2$.

According to (64) this corresponds with a yield stress of

$$\tau_y\ G^5 = 21.8\ N/m^2 \qquad (m = 5) .$$

This value should correspond with the yield stress whereby the dependence of U_* on $\tau_y\ G^m$ changes strongly. However, from figure 15, we see that this value is much too high. In conclusion we may say that the physical properties of the bed in series II have changed so much that Migniot's data are not applicable.

Nevertheless we have made an attempt to fit series II. By trial we found that if the value of B_1 and B_2 in (62) are lowered, a slightly better fit could be obtained. In particular for $B_1 = 1$ and $B_2 = 2$ and $m = 5$, it follows from (24) that $q_1 = 0.1$ and $q_2 = 0.2$.

By fitting two points in the first region of series II (figure 18) and another point in region 2 we obtain for A_1 , A_2 in (62) in M.K.S. units :

(70) $$A_1 = 1.7 \times 10^{-6} \quad , \quad A_2 = 19.9 \times 10^{-6} .$$

By using $D_{v_1} = 1.7 \times 10^{-11}\ m^2/s$ we find now from (63) and (24) that :

$$p_1 = 0.036 .$$

With these values the yield stress at the top of the sediment bed which separates region 1 from region 2 follows from (64) as $\tau_y = 2.2\ N/m^2$. This value corresponds nicely with the breaking point observed by Migniot (fig. 15). The value of p_2 can now be determined from the relation

$$U_* = p_1\ \tau_y^{q_1} = p_2\ \tau_y^{q_2}$$

which holds true at the breaking point where region 1 and 2 meet, as follows from (22). We obtain $p_2 = 0.033$.

The diffusion coefficient in region 2 follows now from (70), (63) and (24) as $D_{v_2} = 370 \times 10^{-11}$ which is 100 times larger than for series 1. The equations for the erosion flux in series II are in M.K.S. units :

$$J_1 = 1.7 \times 10^{-6}\ (\tau - 0.34)\ \tau^{\frac{1}{2}} \qquad 0.34\ N/m^2 \leq \tau \leq 1.48\ N/m^2$$

$$J_2 = 19.9 \times 10^{-6}\ (\tau^{0.5} - 1.12)\ \tau^{\frac{1}{2}} \qquad \tau \geq 1.48\ N/m^2 .$$

These give a good description as shown in figure 18.

References

BAGNOLD, R.A., (1956). *Phil. Trans. Roy. Soc. London, A 249.*

BÖHNECKE, G., (1922). Salzgehalt und Strömungen der Nordsee. Veröff. Inst. Meeresk. Univ. Berl., Neue Folge A., *Geog.-Naturwiss. Reihe N° 10,* 1-34.

BOWDEN, K.F., (1965). *J. Fluid Mech., 21,* 83.

CARRUTHERS, J.N., (1935). The flow of water through the Straits of Dover, *Fishery Investigations,* Series N° 2, 1-67.

CARTWRIGHT, D.E., (1961). *J. Institute Navigation, 14,* 130-151.

ELDER, J.W., (1959). *J. Fluid Mech., 5,* 544.

ELSKENS, I., (1974). *Some aspects of the dynamic behaviour of metallic and other pollutants in the water column and the associated sectors,* Part 4, Sediments, in Math. Modelsea I.C.E.S. Hydrography Committee, C.M. 1974 - C : 1, 439-450.

FUJITA, H., (1962). *Mathematical Theory of Sedimentation Analysis*, Academic Press, N.Y.

GODIN, G., (1966). *The tides in the Labrador Sea, Davis Strait and Baffin Bay*, Marine Science Branch Manuscript Report Series, N° 2, Ottawa.

GULLENTOPS, F., (1974). *Detrital Sedimentology in the Southern Bight of the North Sea*, in Math. Modelsea, I.C.E.S. Hydrography Committee, C.M. 1974 - C : 1, 55-80.

HILL, H.W., (1973). *Currents and water masses*, in *North Sea Science*, edited by E. Goldberg, MIT University Press, 17-42.

KALLE, K., (1949). *Die natürlichen Eigenschaften der Gewässer*, in *Handbuch der Seefischerei Nordeuropas*. Vol. 1, Part 2, edited by Schweizerbart, Stuttgart.

KLINE, S.J., REYNOLDS, W.C., SCHRAUB, F.A. and RUNSTADLER, P.S., (1967). *J. Fluid Mech., 30*, 741.

LEAVASTU, T., (1963). *Serial Atlas of Marine Environment*, Amer. Geoph. Soc. Publ.

McCAVE, I.N., (1972). *Transport and Escape of Fine Grained Sediment from Shelf Area*, in *Shelf Sediment Transport Process and Pattern*, Dowclen-Hutchinson and Ross Publ.

MIGNIOT, C., (1968). *La Houille Blanche, 7*, 591.

MONIM, A.S. and YAGLOM, A.M., (1965). *Statistical Fluid Mechanics*, MIT Press, Cambridge, Mass.

NIHOUL, J.C.J., (1974). *Advances in Geophysics, 18 A*, 331.

NIHOUL, J.C.J., (1975a). *Modelling of Marine Systems*, Elsevier Publ., Amsterdam.

NIHOUL, J.C.J., (1975b). *Application of Mathematical Models to the Study, Monitoring and Management of the North Sea*, in *Ecological Modelling in a Resource Management Framework*, Resources for the Future, Washington D.C.

NIHOUL, J.C.J., (1975c). *Effect of the tidal stress on mud deposition in the Southern Bight of the North Sea*, Proc. 2nd Annual Meeting of the European Ceophysical Society, Trieste 20-26 Sept. 1974.

NIHOUL, J.C.J., (1975d). *Mesoscale secondary flows. Implications in the chemical and biochemical dynamics of the Southern Bight of the North Sea*, Liège 6th Coll. Ocean Hydrodyn., *Mém. Soc. Roy. Sci. Liège.*

NIHOUL, J.C.J. and ADAM, Y., (1974). Programme national sur l'environnement physique et biologique, C.I.P.S., *N 36*.

NIHOUL, J.C.J. and RONDAY, F.C., (1975). *Tellus*, *27*, 5.

OTTO, L., (1970). *The mean residual transport in the Southern North Sea*, I.C.E.S., C.M. 1970 - C : 21.

PARTHENIADES, E., (1965). *J. Hydraulics Div.*, *91*, HY 1 4204

PARTHENIADES, E., (1972). *Results of recent investigations on erosion and deposition of cohesive sediments*, in *Sediments*, edited by Hsich Wen Shen, Fort Collins, U.S.A.

PODAMO, J., (1974). *Aspects of dynamic biology in the Southern Bight of the North Sea*, in Math. Modelsea, I.C.E.S. Hydrography Committee, C.M. 1974 - C : 1.

TAYLOR, G.I., (1922). *Proc. London Math. Soc.*, *20*, 148.

TAYLOR, G.I., (1953). *Proc. Roy. Soc.*, *A 219*, 186.

TAYLOR, G.I., (1954). *Proc. Roy. Soc.*, *A 223*, 446.

WOLLAST, R. and VAN DER BORGHT, (1974). *Model of mass transfer in a benthic boundary layer submitted to physical and biological perturbations*, Nato Science Committee Conf., Les Arcs, France.

WYRTKI, K., (1954). *Deutsche Hydrog. Zeit*, *7*, 91.

YALIN, M.S., (1972). *Mechanics of Sediment Transport*, Pergamon Publ., Oxford.